FROM GLOBULAR CLUSTERS TO TIDAL DWARFS: STRUCTURE FORMATION IN THE TIDAL TAILS OF MERGING GALAXIES[1]

Karen A. Knierman,[2] Sarah C. Gallagher,[3] Jane C. Charlton, and Sally D. Hunsberger

Department of Astronomy and Astrophysics, 525 Davey Laboratory, Pennsylvania State University, University Park, PA 16802;
kak@astro.psu.edu, gallsc@astro.psu.edu, charlton@astro.psu.edu, sdh@astro.psu.edu

Bradley Whitmore

Space Telescope Science Institute, 3700 San Martin Drive, Baltimore, MD 21218; whitmore@stsci.edu

Arunav Kundu

Department of Physics and Astronomy, Michigan State University, East Lansing, MI 48824; akundu@pa.msu.edu

J. E. Hibbard

National Radio Astronomy Observatory, 520 Edgemont Road, Charlottesville, VA 22903; jhibbard@nrao.edu

and

Dennis Zaritsky

Steward Observatory, University of Arizona, 933 North Cherry Avenue, Tucson, AZ 85721; dennis@ngala.as.arizona.edu

ABSTRACT

Using V and I images obtained with the Wide Field Planetary Camera 2 (WFPC2) of the *Hubble Space Telescope*, we investigate compact stellar structures within tidal tails. Six regions of tidal debris in the four classic "Toomre sequence" mergers: NGC 4038/39 ("Antennae"), NGC 3256, NGC 3921, and NGC 7252 ("Atoms for Peace") have been studied in order to explore how the star formation depends on the local and global physical conditions. These mergers sample a range of stages in the evolutionary sequence and tails with and without embedded tidal dwarf galaxies. The six tails are found to contain a variety of stellar structures, with sizes ranging from those of globular clusters up to those of dwarf galaxies. From V and I WFPC2 images, we measure the luminosities and colors of the star clusters. NGC 3256 is found to have a large population of blue clusters ($0.2 \lesssim V-I \lesssim 0.9$), particularly in its western tail, similar to those found in the inner region of the merger. In contrast, NGC 4038/39 has no clusters in the observed region of the tail, only less luminous point sources likely to be individual stars. NGC 3921 and NGC 7252 have small populations of clusters along their tails. A significant cluster population is clearly associated with the prominent tidal dwarf candidates in the eastern and western tails of NGC 7252. The cluster-rich western tail of NGC 3256 is *not* distinguished from the others by its dynamical age or by its total H I mass. However, the mergers that have few clusters in the tail all have tidal dwarf galaxies, while NGC 3256 does not have prominent tidal dwarfs. We speculate that star formation in tidal tails may manifest itself either in small structures like clusters along the tail or in large structures such as dwarf galaxies, but not in both. Also, NGC 3256 has the highest star formation rate of the four mergers studied, which may contribute to the high number of star clusters in its tidal tails.

Key words: galaxies: individual (NGC 3256, NGC 3921, NGC 4038/39, NGC 7252) —
galaxies: interactions — galaxies: star clusters

1. INTRODUCTION

There is growing evidence that massive young compact star clusters form in many different environments. Old globular clusters, like those seen in the Milky Way, presumably form in the early stages of galaxy formation. Recently, young compact clusters were discovered to be forming in several environments: starburst galaxies (Meurer et al. 1995), barred galaxies (Barth et al. 1995), some spiral disks (Larsen & Richtler 1999), the inner regions of mergers (Holtzman et al. 1992; Whitmore et al. 1993, 1999b; Schweizer et al. 1996; Miller et al. 1997; Zepf et al. 1999), and in the space between galaxies in compact groups (Gallagher et al. 2001). Finding common characteristics between these environments may allow us to identify the mechanism that causes gas clouds to collapse and efficient star formation to begin (e.g., Jog & Solomon 1992). Also, there may be differences from environment to environment that lead to different types of "packaging" of new stars, from isolated stars, to small groups, to globular clusters, to stellar associations, to dwarf galaxies. To understand the underlying conditions responsible for the formation of these structures, it is important to identify the different environments in which they form.

Star clusters tend to form wherever vigorous star formation occurs and, especially, in starbursts triggered by galaxy interactions and mergers (Schweizer 1998). Studies with the *Hubble Space Telescope* (*HST*) of several mergers and merger remnants show a large number of young clusters in

[2] Current address: Steward Observatory, University of Arizona, 933 North Cherry Avenue, Tucson, AZ 85721; kknierman@as.arizona.edu.

[3] Current address: Center for Space Research, Massachusetts Institute of Technology, 77 Massachusetts Avenue, Cambridge, MA 02139; scg@space.mit.edu.

the inner regions of the galaxies (Whitmore et al. 1993, 1999b; Whitmore & Schweizer 1995; Schweizer et al. 1996; Miller et al. 1997; Zepf et al. 1999). The clusters have effective radii comparable to, but perhaps slightly larger than, the old globular clusters in the Milky Way. Their luminosity functions are best described as power laws ($\alpha \sim -2$), when expressed as the number of clusters per luminosity bin. While this is similar to the luminosity function of globular clusters in the Milky Way for masses greater than $\sim 10^5\ M_\odot$ (Harris & Pudritz 1994), merging galaxies have many more low-mass clusters than are found in galaxies with old globular cluster populations. This disparity could indicate a difference in the cluster formation process in primordial galaxies as compared with modern merger remnants, or it could simply indicate that evolution of the luminosity function has occurred because of fading and selective disruption (Zhang & Fall 1999).

Bridges and tails may also form during strong tidal interactions involving disk galaxies (Toomre & Toomre 1972; Barnes 1988). These tidal features have blue $UBVR$ colors (e.g., $B-V = 0.53 \pm 0.13$, from Schombert, Wallin, & Struck-Marcell 1990; see also Weilbacher et al. 2000), and regions of [O II] and Hα line emission have been found within the tails (Schweizer 1978; Mirabel, Dottori, & Lutz 1992; Duc & Mirabel 1998, 1999; Iglesias-Páramo & Vílchez 2001; Weilbacher, Duc, & Fritze-v. Alvensleben 2003). The inferred ages of the young stars and giant H II regions are much less than the dynamical age of the tails, indicating that star formation is occurring within the tails.

Several factors may influence star formation within tidal tails. First, the stage of the merger may be important. Second, 21 cm neutral hydrogen (H I) observations indicate that tails are gas rich (Yun, Ho, & Lo 1994; Hibbard et al. 2001b) and that the evolution of the H I may play a role in the star formation history. Many tidal tails have associated H I that is falling back toward the center into the remnant. This infall of gas may enable star formation to continue for timescales on the order of 1 Gyr after tail formation (Hibbard & Mihos 1995). Finally, tidal dwarf galaxies are found in tidal tails in a variety of environments, particularly at the ends of the tails (Mirabel, Dottori, & Lutz 1992; Duc & Mirabel 1994; Hunsberger, Charlton, & Zaritsky 1996). These same tails that form tidal dwarfs may or may not form smaller stellar structures such as star clusters. Recent results from the early release observations of the Advanced Camera for Surveys (ACS) on the *HST* have shown young star clusters in the tidal tails of UGC 10214 (the "Tadpole"; Tran et al. 2003; de Grijs et al. 2003) and NGC 4676 (the "Mice"; de Grijs et al. 2003).

This paper focuses on the occurrence of star clusters in the tidal tails of merging galaxies. New *V*- and *I*-band observations of the tidal tails of four merging pairs obtained with *HST* WFPC2 are presented. These are compared with previous observations of the inner regions of the same galaxies and to each other, in order to consider the factors that influence the nature of the stellar systems that form in the tails. The four mergers chosen for this study span a range of dynamical states and tails with and without embedded tidal dwarf galaxies.

The four systems in this study were chosen from the "Toomre sequence" (Toomre 1977) of ongoing mergers. This sequence is an optically selected ensemble of strongly interacting galaxies representing a suggested evolutionary sequence of disk-disk mergers, based on their stellar tidal tail lengths and the separation of the two nuclei (Toomre 1977). The four systems chosen for this study span the entire range of the sequence, from strongly disturbed, but separate, disks likely to merge (NGC 4038/39, the "Antennae"), to nearly fully merged disks (NGC 3256), to fully merged systems with single nuclei and relaxed stellar profiles (NGC 3921 and NGC 7252, "Atoms for Peace).

In the following, § 2 describes the *HST* observations and their reduction, object selection, and photometry. Section 3 presents the four mergers in separate subsections, with each having a description of the observations, inner regions, and results and a discussion. Then § 4 compares the results for the different mergers and summarizes the main conclusions.

2. OBSERVATIONS AND REDUCTIONS

2.1. *Observations*

Observations of six tidal tails were obtained with the *HST* WFPC2 during the period 1998 November to 1999 October, as listed in the journal of observations in Table 1. Total integration times ranged from 1000 to 2000 s in *V* (F555W filter) and *I* (F814W filter). The integrations were chosen to obtain images to a depth similar to the observations of the inner regions. A gain of $7\ e^-\ \mathrm{ADU}^{-1}$ was used in all cases. At least two separate exposures in each filter were obtained to facilitate removal of cosmic rays. The positions of the WFPC2 field of view is superposed on optical images of the four mergers in Figure 1. The six *V*-band images are presented in Figures 2–7.

Pairs of exposures were taken for all systems except NGC 3256 The exposures were offset by 0″.25 (i.e., 2.5 pixels on the Wide Field Camera [WF] and 5.5 pixels on the Planetary Camera [PC]). Pipeline-reduced images for each filter were averaged and cleaned using the IRAF[4] task GCOMBINE. The task COSMICRAYS was used to remove hot pixels.

2.2. *Object Detection*

Objects in the images were detected using the DAOFIND task in the DAOPHOT package using a threshold of 2.0 counts per object, finding objects greater than 2 σ above the local sky background. The noise was determined from the

---

[4] IRAF is distributed by the National Optical Astronomy Observatory, which is operated by AURA, Inc., under contract to the NSF.

TABLE 1
JOURNAL OF OBSERVATIONS

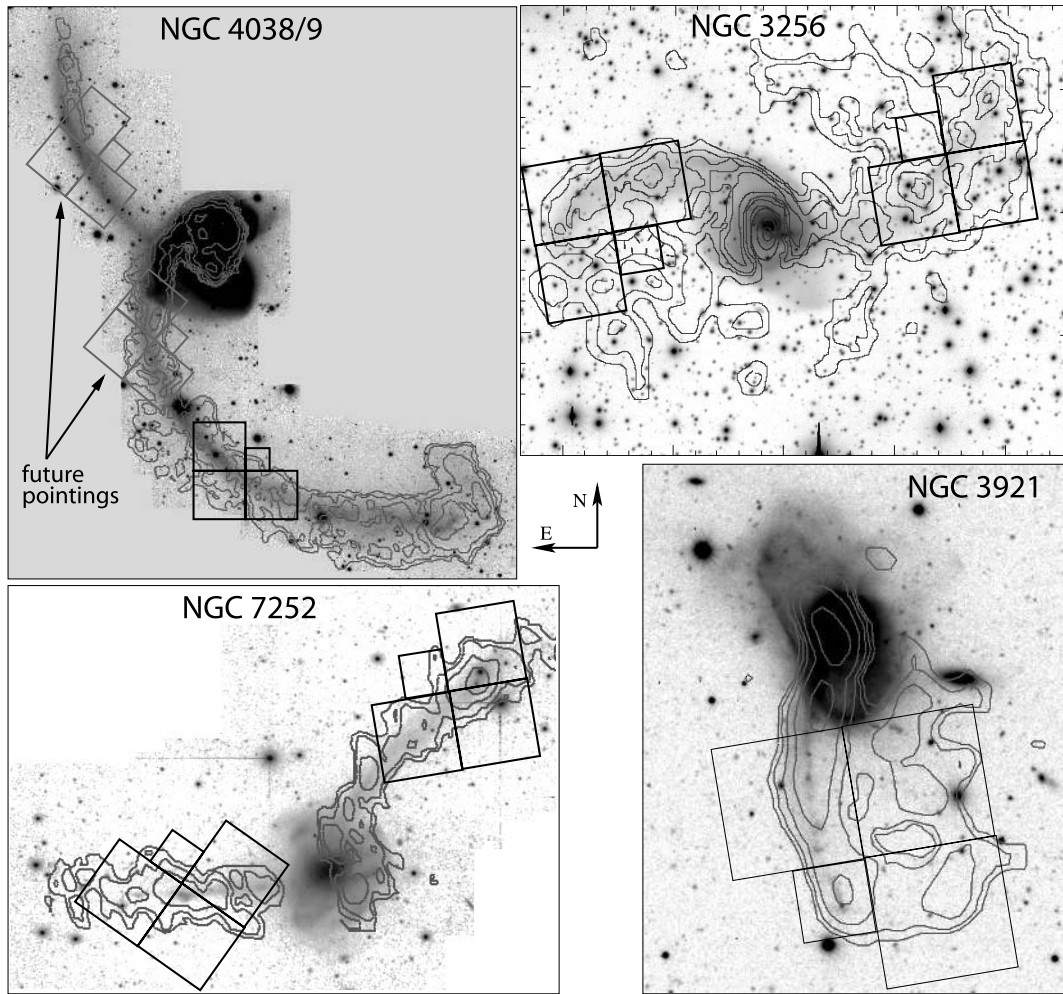| Tidal Tail	Filter	Time (s)	Date
NGC4038	F555W	2000	1999 Feb 22
	F814W	1800	1999 Feb 22
NGC3256W..............	F555W	1000	1999 Mar 24
	F814W	1000	1999 Mar 24
NGC3256E...............	F555W	1000	1999 Oct 11
	F814W	1000	1999 Oct 11
NGC3921S	F555W	1800	1999 Apr 30
	F814W	1600	1999 Apr 30
NGC7252W..............	F555W	2000	1998 Nov 18
	F814W	1800	1998 Nov 18
NGC7252E...............	F555W	2000	1999 Aug 29
	F814W	1800	1999 Aug 29

FIG. 1.—*Top left*: Optical image in *BVR* of early stage remnant NGC 4038/39 (Antennae) from the Cerro Tololo Inter-American Observatory (CTIO) 0.9 m telescope with integrated H I line emission, shown as overlaid contours taken with the VLA C and D configurations (Hibbard et al. 2001a). Shown are the *HST* WFPC2 field of view of our 1999 February 22 observations (*black boxes*) and our two later observations (*gray boxes*; not analyzed here). *Top right*: Optical image of NGC 3256 from University of Hawaii 88 inch (2.2 m) telescope *R* band. The *HST* WFPC2 fields of view of our observations are indicated by the black boxes. H I data have been obtained at the Australia Telescope Compact Array (English et al. 2003). *Bottom left*: Optical image of NGC 7252, from the CTIO 4 m R_j band, with H I contours overlaid (Hibbard & van Gorkom 1996). *Bottom right*: Optical image of NGC 3921, KPNO 0.9 m *R*-band image, with integrated H I line emission, shown in overlaid contours taken with the VLA C plus D configurations (Hibbard & van Gorkom 1996).

sky annulus of 5–8 pixels around each object identified by DAOFIND, and only objects with a signal-to-noise ratio per object greater than 3 were retained. For images with multiple exposures, the objects were detected separately in each pointing. Then the two source lists were matched using the offsets calculated from bright stars. Only those sources with detections in both the *V* and *I* filters were retained.

Only pointlike sources are of interest in this paper, since extended objects will be addressed in a future study. In addition to possible star clusters, this method detects foreground stars and compact background galaxies. We use a classification based on the *V−I* color and a structural parameter. To obtain a sample of possible star clusters, we keep only those sources with *V−I* < 2.0. Old, metal-poor globular clusters in the Milky Way have *V−I* ∼ 1 (Reed, Hesser, & Shawl 1988), so this cut would not exclude old clusters. The most metal-rich clusters, from observations of the Milky Way and nearby elliptical galaxies, have *V−I* < 1.5 (Peterson 1993; Ajhar, Blakeslee, & Tonry 1994; Whitmore et al. 1995; Kundu & Whitmore 2001a, 2001b). Stellar population

models by Lee, Lee, & Gibson (2002), which take into account the effect of the horizontal branch on colors show that even solar metallicity globular clusters only have *V−I* ∼ 1.2–1.3. Also, only those sources with $V_{err} < 0.25$ were retained.

As in Whitmore et al. (1993) and Miller et al. (1997), we calculated the concentration index, the difference in *V* magnitude between an aperture of 0.5 pixel radius and an aperture of 3.0 pixel radius, denoted by $\Delta_V (0.5 - 3)$. A sky annulus of 6–9 pixels was used to subtract the background. For each system, we used a different concentration index. In the NGC 3256 images, we classified objects with $\Delta_V (0.5 - 3) > 2.4$ as diffuse and removed them from the sample. The cutoff for the concentration index was raised to 3.0 for NGC 4038/39, the closest system, to avoid eliminating any possible clusters.

For NGC 3921 and NGC 7252, we modified the above photometry method to probe deeper apparent magnitudes for comparison with the central regions and larger-sized objects, such as the stellar associations found close to the
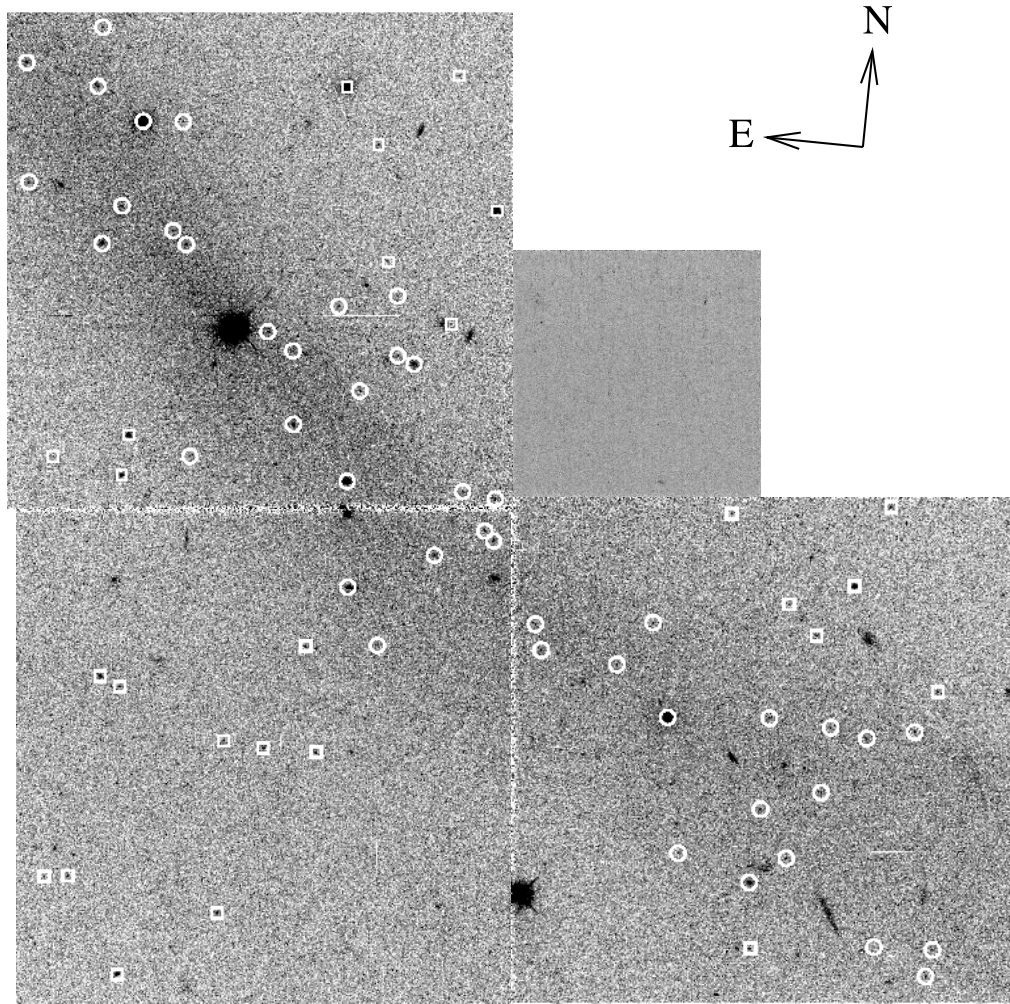
FIG. 2.—*HST* WFPC2 image of the NGC 4038/39 (Antennae) southern tail taken with F555W (*V*) filter. Sources inside (*circles*) and outside (*squares*) of the tail are indicated. Sources within the tail are likely to be individual stars and not clusters.

central regions of NGC 3921 (Schweizer et al. 1996). For these images we used DAOFIND with the threshold set at 1.5, rather than 2.0 as above. The signal-to-noise ratio was calculated again, this time using a cutoff of 1.5 per object. As above we retained sources with $V-I < 2.0$ and $V_{err} < 0.25$. There was no cutoff for the concentration index. By removing the size criteria for objects in these mergers, we retained more diffuse sources that we could compare with the stellar associations from Schweizer et al. (1996).

For each tail, a region in the *V*-band image was manually identified as "in tail," corresponding to contiguous regions with ∼1 count (DN) above the background (corresponding to a *V* magnitude surface brightness of 24.3–25.7 mag arcsec^{-2}, according to the specific tail). All other regions were designated as "out of tail." In Figures 2–7, in-tail point sources are indicated by circles, while out-of-tail point sources are indicated by squares.

2.3. *Completeness*

Figure 8 shows the completeness fraction on the wide-field chips for the observations of NGC 3256W. The completeness was determined by adding 10,000 stars (100 at a time to avoid

crowding) using the ADDSTAR program within the DAOPHOT package. The surface brightness of the tail is so low (∼1 DN above the background) that a single background level is sufficient for characterizing the completeness fractions, rather than the multiple curves used in other studies with a wide variety of backgrounds (e.g., Whitmore et al. 1999b). We find that the completeness fraction reaches ∼50% at $V = 25.8$, or 25.4 corrected for foreground extinction, consistent with our visual estimate of the completeness correction from the color-magnitude diagram (CMD) for NGC 3256W (see Fig. 11). Comparison of the CMDs indicates that the completeness limits for NGC 3921 and NGC 4038/39 are similar to that of NGC 3256. For NGC 7252, our slightly relaxed detection criterion (see § 2.2) yields a slightly deeper completeness limit, by ∼0.2 mag.

For several reasons few sources were detected on the PC chip in any of the fields (eight in the NGC 3256W PC, two in the NGC 3256E PC, and none in any others). First, the fields were positioned for maximal total coverage of the tail regions, from which it follows that the tails do not pass through the PC chip. Second, the area covered by the PC chip is smaller than a single WF chip. Finally, in the PC chip the light is spread over a larger number of pixels, but the
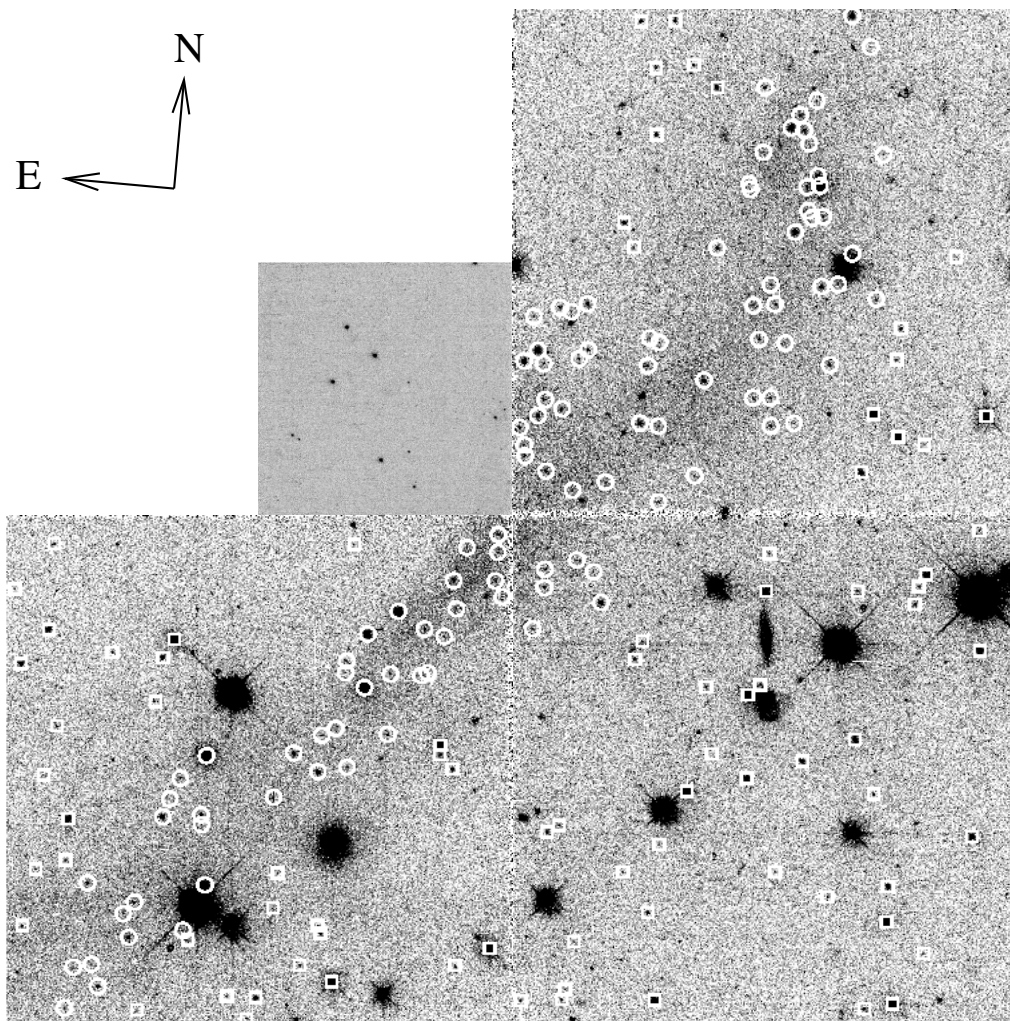
FIG. 3.—Same as Fig. 2, but for the NGC 3256 western tail. The majority of sources within the tail are likely to be clusters; note the large number.

read noise is the same per pixel. We are working in a regime in which read noise is important, thus the detection limit is not as faint for the PC as for the WF (see Whitmore et al. 1999b for a similar comparison). Therefore, only WF observations will be discussed in this study. The PC sources have not been plotted in Figures 2–7.

2.4. *Photometry*

Photometric zero points were adopted from Table 28.1 of version 3 of the *HST* Data Handbook (Voit 1997). The Holtzman et al. (1995) photometric transformation corrections were applied (to convert from the *HST* filter system to the Johnson-Cousins system).

Aperture photometry was performed on all pointlike objects in the cleaned images using the PHOT task in the APPHOT package. The radii of the object aperture, the inner boundary of the background annulus, and the outer boundary were 2, 5, and 8 pixels, respectively, for the WF. For all fields, the aperture corrections $V = 0.28$ and $I = 0.31$ were adopted. These were an average of those derived for stars in the three WF chips for NGC 1700 and NGC 3610 (Whitmore et al. 1997), which were calibrated using point sources in the NGC 5139 (ω Cen) and NGC 6752 fields. Ideally, we would have used cluster candidates

in our own fields to determine aperture corrections; however, this procedure was subject to large uncertainties because of a lack of sufficiently bright sources. For the best case, WF2 in the NGC 3256W image, nine bright stars were used to determine corrections of 0.276 ± 0.014 in V and 0.293 ± 0.006 in I. These are consistent with our adopted values. For the nearest pair, using stellar aperture corrections (instead of clusters) introduces a systematic error of only a couple hundredths of a magnitude, insignificant for the purpose of this study.

The foreground extinction due to the Galaxy was corrected for each pair using the A_B values from Schlegel, Finkbeiner, & Davis (1998) and the reddening curve from Mathis (1990). The A_B values for each merger are listed in Table 2. We corrected for nonoptimal charge transfer efficiency (CTE) using the formulae of Whitmore, Heyer, & Casertano (1999a).

3. THE FOUR MERGING PAIRS

For each of the mergers we summarize past observations of the inner regions, present new *HST* observations, and discuss our results. Figure 1 shows optical images of the four mergers with H I contours and with the locations of the six
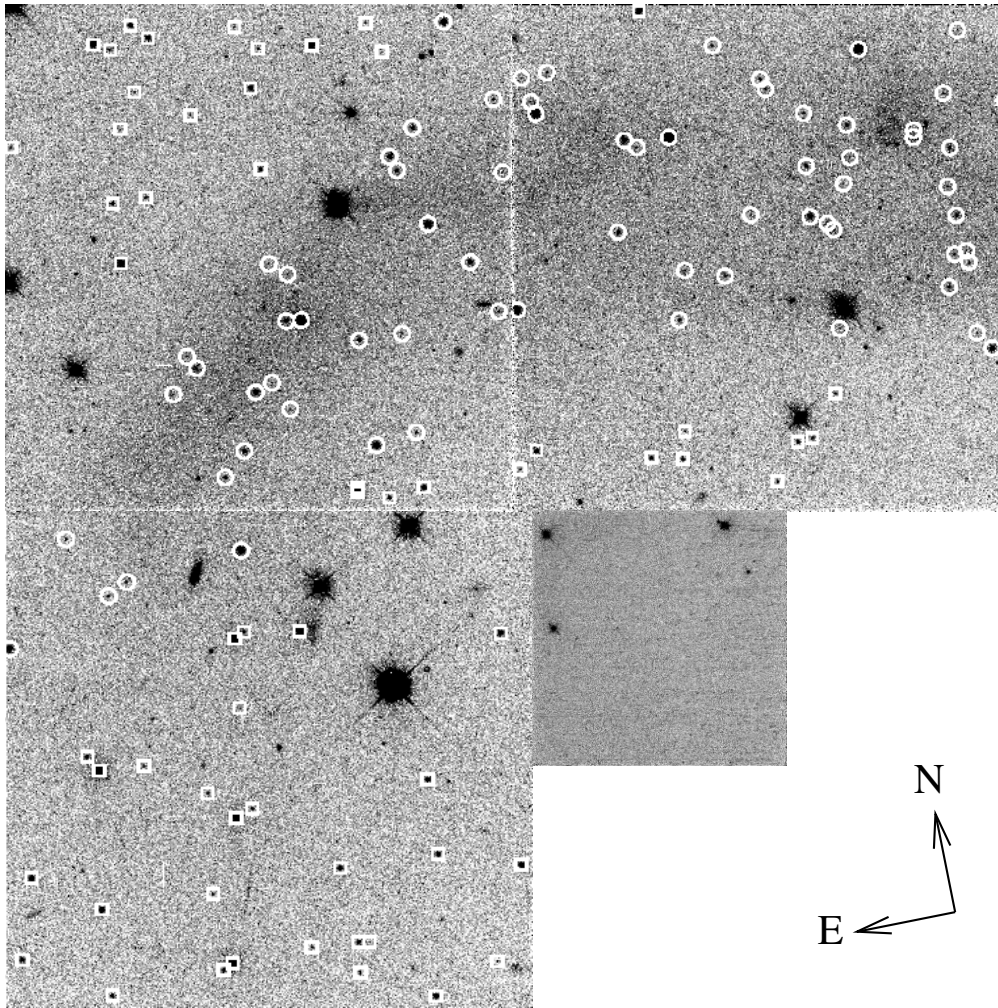
N

E

Fig. 4.—Same as Fig. 2, but for the NGC 3256 eastern tail

observed WFPC2 fields superposed. Table 2 presents a comparison of tail properties including the velocity of merger, distance modulus, extinction in B magnitudes (A_B), length from the central region along the tail to the position at which the image begins (l), physical scale of the tail region encompassed in the image (Δl), absolute magnitude for the 50% completeness limit ($M_{V,50\%}$), H I mass of the tail ($M_{\rm H\,I,tail}$), and the approximate age of the tail (the projected length of the tail divided by the rotational or escape velocity). The mergers are discussed in increasing order of their place in the Toomre sequence.

3.1. NGC 4038/39 (The Antennae)

The Antennae is one of the best known and earliest modeled merger systems (Toomre & Toomre 1972; van der Hulst 1979). It is the nearest of the four mergers in this study (see Table 2). Its long, nearly symmetric crossed tidal tails and still-separate nuclei indicate a relatively young, strongly interacting merger; see Figure 1 for an optical image. The southern tail is longer than the northern one and features a putative dwarf galaxy at the tip (Schweizer 1978; Mirabel et al. 1992). Images in Hα of NGC 4038/39 show vigorous

TABLE 2
SUMMARY OF TIDAL TAIL PROPERTIES

Tidal Tail	Velocity (km s^{-1})	Distance Modulus (mag)	A_B[a] (mag)	l (kpc)	Δl (kpc)	$M_{V,50\%}$[b] (mag)	$M_{\rm H\,I,\,tail}$ $M_\odot$	Tail Age (Myr)
NGC 4038..................	1439	31.4	0.200	30	20	−5.8	2.0×10^8	420
NGC 3256W	2820	32.9	0.524	15	40	−7.5	2.2×10^9	400
NGC 3256E	2820	32.9	0.524	15	30	−7.5	1.4×10^9	400
NGC 3921S................	6021	34.5	0.062	0	45	−8.7	4.3×10^9	460
NGC 7252W	4828	34.0	0.130	20	50	−8.1	2.2×10^9	730
NGC 7252E	4828	34.0	0.130	0	60	−8.1	1.5×10^9	730

[a] From Schlegel et al. 1998.
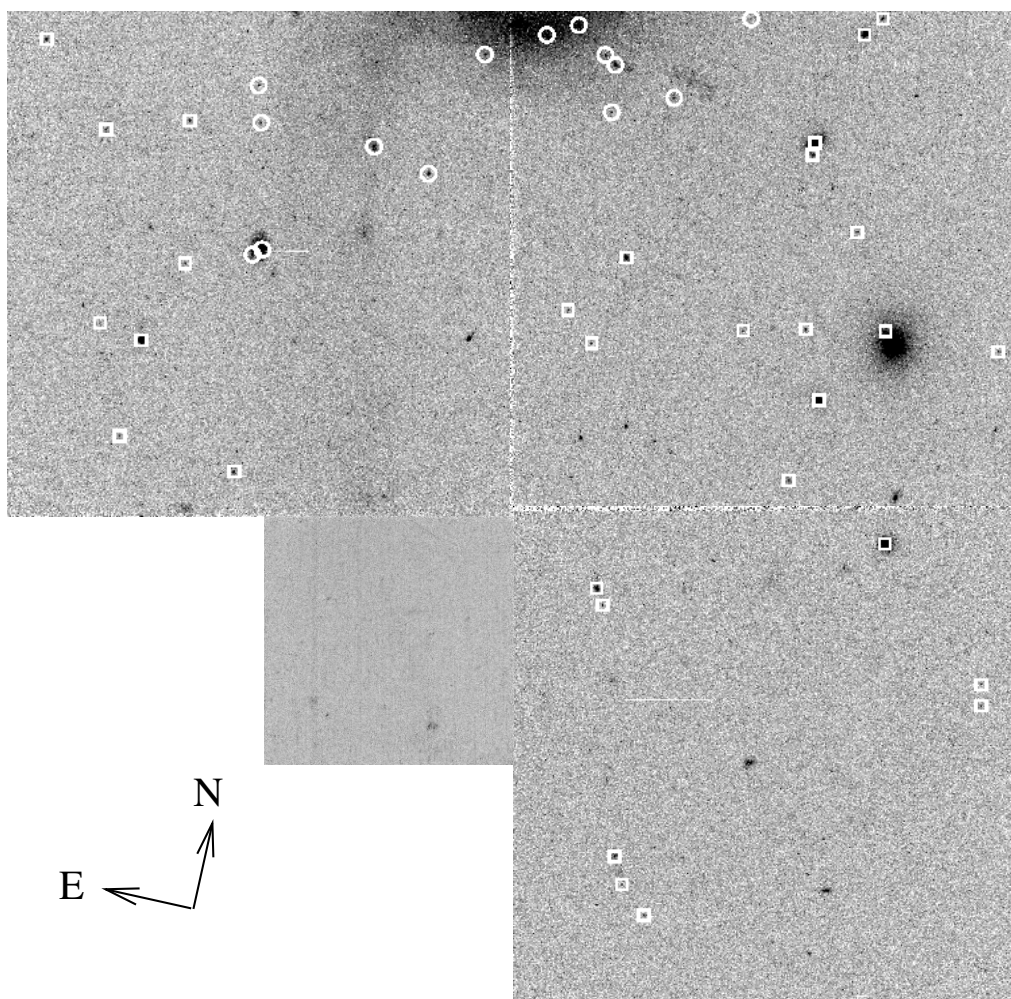[b] Limiting magnitude for ~50% completeness.

Fig. 5.—Same as Fig. 2, but for the NGC 3921 southern tail

star formation within the main disks (Whitmore & Schweizer 1995). The optical spectrum, with a blue continuum and strong emission lines, is indicative of an active star-forming galaxy. The equivalent width of the Hα line is 2–3 times higher than the normal average of $\sim$25 Å in an average Sb or Sc galaxy, categorizing NGC 4038/39 as a starburst galaxy (Kennicutt 1992).

The southern tail is rich in H I, while the northern is H I–poor. H I contours overlay the optical image in Figure 1 (from Hibbard et al. 2001a). At the end of the southern tail lie at least three H II regions. A spectrum from Mirabel et al. (1992) shows that this region has a low O/H abundance, which is typical of dwarf galaxies. The region at the tip of the tail also shows a high concentration of H I (van der Hulst 1979; Hibbard et al. 2001a).

We use the maximum projected tail length of 65 kpc (Schweizer 1978, corrected for our adopted distance) and the disk rotation speed of 150 km s^{-1}, inferred from the Fabry-Perot observations of Amram et al. (1992) and corrected for disk inclination, to infer an interaction age of 65 kpc/150 km s^{-1} = 420 Myr. This age, measured from orbital periapse when the tails were launched, is in excellent agreement with the best match time of 450 Myr from the numerical model of NGC 4038/39 run by Barnes (1988). It is also remarkably close to the age of the population of 500 Myr old globular clusters found by Whitmore et al.

(1999b; see also Fritze-v. Alvensleben 1998), supporting the hypothesis that this globular cluster population formed around the time when the tails were first ejected (Whitmore et al. 1999b).

3.1.1. *Inner Region*

Whitmore et al. (1999b) found young globular clusters in the inner regions of the Antennae. More than 14,000 point-like objects were identified in the field, of which most were probably young stars formed in the merger. Depending on selection criteria, the number of young compact star clusters is between 800 and 8000. Remaining sources are individual supergiant stars, also in the Antennae. The luminosity function is composed of two power-law segments with a bend at $M_V \sim -10.4$. The median effective radius of the young clusters is 4 ± 1 pc, just slightly larger than the 3 pc radius for Milky Way globular clusters (van den Bergh 1996). The ages of the young clusters range from less than 5 Myr up to 100 Myr. There are also populations of intermediate age (500 Myr) and of old globular clusters (Whitmore et al. 1999b).

3.1.2. *Observations of the Southern Tail*

Three observations were planned for this merger, but only one has been included in this study. In Figure 1, the
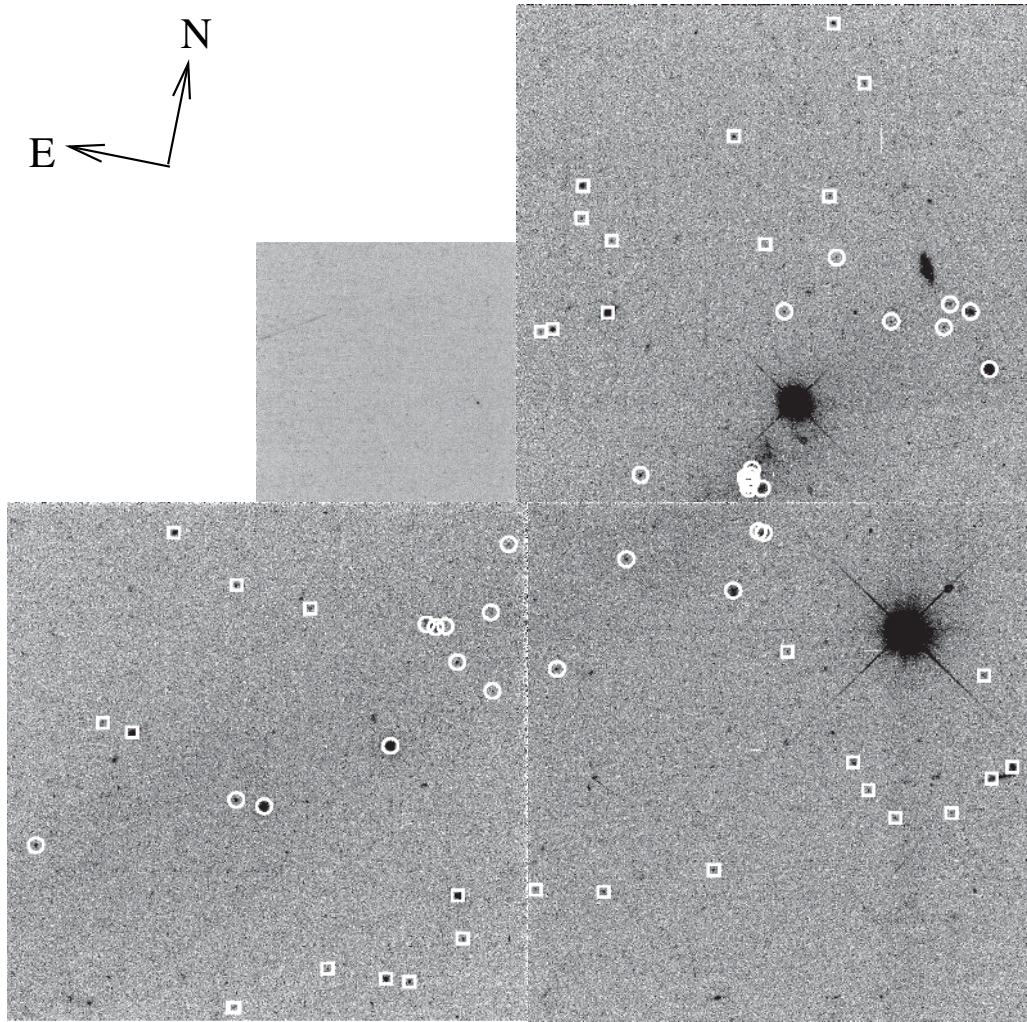
FIG. 6.—Same as Fig. 2, but for the NGC 7252 western tail

WFPC2 field of view is overlaid on an optical image of NGC 4038/39. The WFPC2 image was obtained on 1999 February 22 (see the *V*-band image in Fig. 2). Two later observations, not analyzed here, are indicated by the lighter boxes in the image. At the distance modulus of 31.4 (for $H_0 = 75$ km s^{-1} Mpc^{-1}, as in Whitmore et al. 1999b), the limiting magnitude (50% completeness) of $m_V \sim 25.8$, consistent with our visual estimate of the completeness correction from the CMD, corresponds to an absolute magnitude limit of $M_V \sim -5.8$. Despite the closeness of this merger, a long exposure was obtained (see Table 1) to match the depth of existing images of the inner regions. Therefore, these NGC 4038/39 images are far deeper in absolute magnitude than those of the other mergers presented in this paper. In addition to our image along the middle of the southern tail, *HST* WFPC2 observations of the candidate tidal dwarf galaxy at the tip of the southern tail were obtained by Saviane, Hibbard, & Rich (2003). Their image is 2 mag deeper than our limiting magnitude.

3.1.3. *Results*

A *V*−*I*, *V* CMD is presented in Figure 9. The plot includes only the range $-0.75 < V-I < 2.0$ since we do not expect to see clusters with $V-I > 2.0$. In the inner region of NGC 4038/39, clusters identified by Whitmore et al. (1999b) have an $M_V < -9$ (Fig. 9, *dotted line*) and colors of $0.0 < V-I < 0.6$, with a particular concentration at $-12 < M_V < -10$ and $0.3 < V-I < 0.4$ (Whitmore et al. 1999b). Of the sources in the tail, none lie in the same region of the CMD in which Whitmore et al. (1999b) discover clusters, as shown in Figure 9. The tail sources are fainter and/or redder. The grouping of ~30 sources in the tail CMD falls in the same area as individual stars in the inner region of the Antennae ($M_V > -9$ and $-1.0 < V-I < 1.0$; Whitmore et al. 1999b). Many of these are probably isolated red or blue supergiants. Whitmore et al. (1999b) use *U* and *B* images to help separate stars from the cluster population; however, we have only *V* and *I* images.

Since the in-tail and out-of-tail regions in this field are equal in area, it is noteworthy that there is a larger number of faint sources in the tail regions (42 vs. 24 in the out-of-tail regions). However, there is no significant difference between the distribution of sources in the CMD for sources in and out of the tail (Fig. 9). The probabilities of the magnitudes and colors being drawn from the same distributions are 0.27 and 0.89, respectively, by the Kolmogorov-Smirnov (K-S) test (Press et al. 1986). In Figure 10, the *V*−*I* color is plotted
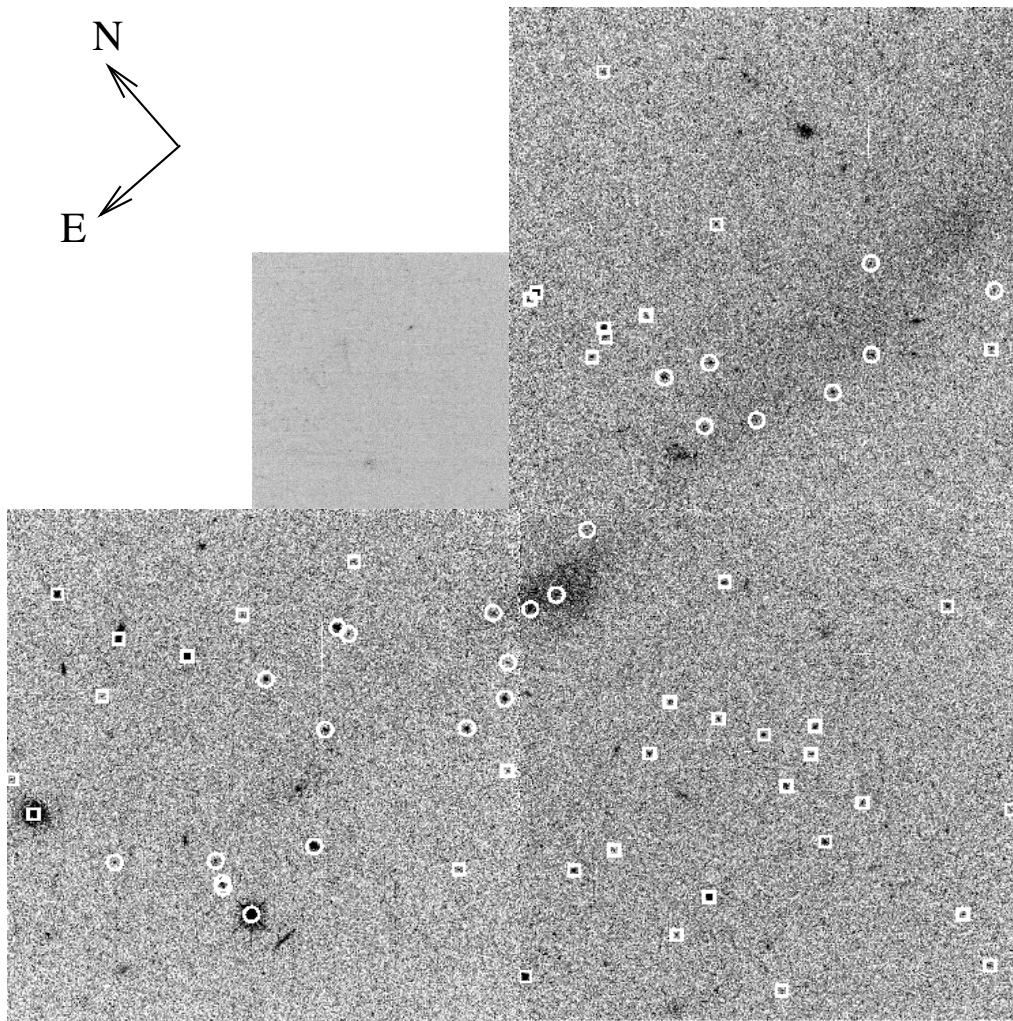
Fig. 7.—Same as Fig. 2, but for the NGC 7252 eastern tail

versus the concentration index, but again there is no difference in the distributions for sources in and out of the tail [P(K-S) = 0.89 for the color and 0.71 for the concentration index distribution].
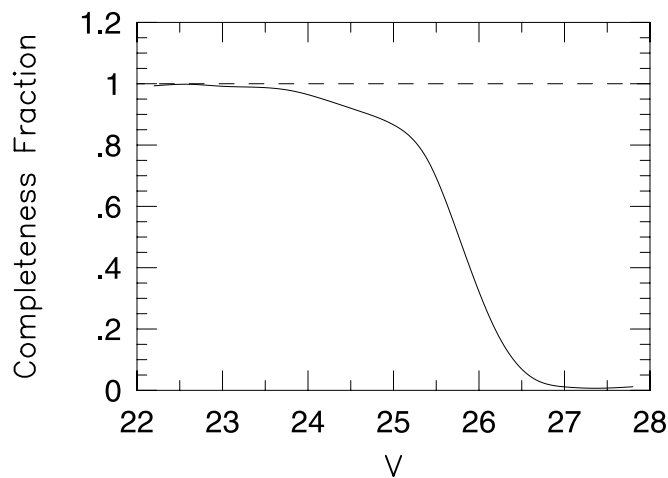

Fig. 8.—Completeness fraction for point sources as a function of the V magnitude, determined by adding artificial sources to the WF images of the NGC 3256 western tail.

3.1.4. *Discussion*

As seen in Figure 2, some of the fainter point sources lie along the optical tail. However, there is an absence of bright ($M_V < -9$) young clusters compared to the inner region. If clusters formed only concurrently with the tail, ~450 Myr ago, they should still be detected in the CMD (see Fig. 9). This is evident since 21 $M_V < -9$ sources of intermediate ages were found by Whitmore et al. (1999b) in their comparable exposure of the body of the NGC 4038/39 merger and its inner tail regions. In fact, many of the fainter sources that we find within the tail may be individual red and blue supergiants, perhaps forming in the tail.

This image was taken ~30 kpc from the inner region and contains ~20 kpc of the southern tail. It is possible that other regions of the tails do have cluster populations. Whitmore et al. (1999b) identified about a dozen objects in the inner part of the southeastern tail, but only one of them was bright enough ($M_V = -9.48$) to be definitively identified as a cluster. Our additional observations include the northern tail, which has less H I by a factor of 5 (van der Hulst 1979; Hibbard et al. 2001a), and another region in the southern tail, which is closer to the inner region. These images provide the opportunity to study the distribution of clusters in the tail and the relationship of the H I content to the characteristics of the cluster population. The candidate
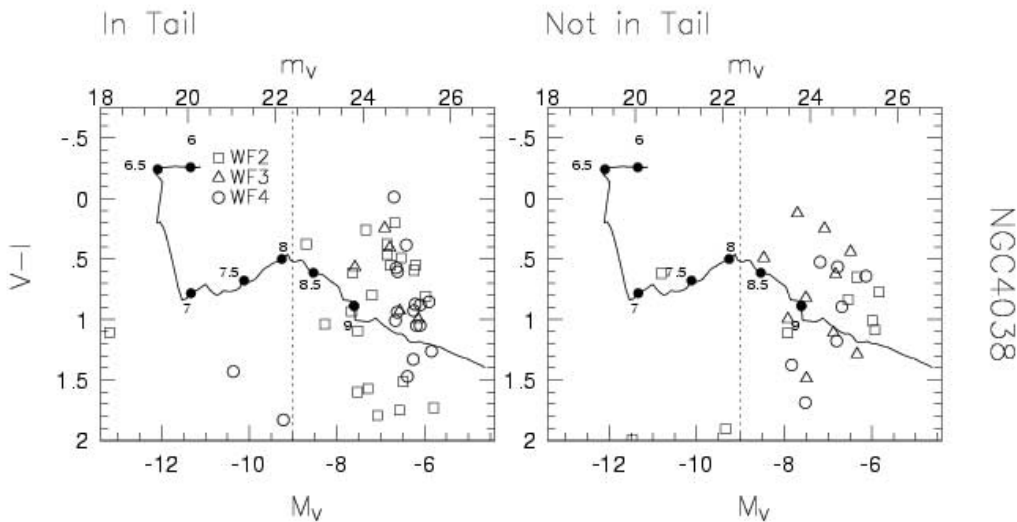
Fig. 9.—CMD for sources in and out of the tail region of NGC 4038. Color $V-I$ is plotted vs. absolute magnitude M_V on the lower horizontal scale and against apparent magnitude V on the upper horizontal scale. The absolute magnitude scale enables comparison between different tails. All sources, both in and out of the tail, with errors in V less than 0.25 mag and with $-0.75 < V-I < 2.0$, are included. Sources coming from the different WF chips are identified by special symbols as indicated in the legend. No corrections have been made for incompleteness. The vertical dashed line indicates a rough boundary such that brighter sources are more likely to be clusters, rather than individual stars. The curve represents the evolutionary track for an instantaneous burst model for a $10^5\,M_\odot$ cluster with solar metallicity and a Salpeter IMF with a $125\,M_\odot$ cutoff, marked with log age in years (Bruzual & Charlot 1993; Charlot et al. 1996). This model would shift by a magnitude horizontally for every factor of 2.5 in mass.

tidal dwarf galaxy at the tip of the southern tail has eight extended young star clusters, five of which are brighter than $M_V = -8.5$, and many young blue stars fainter than $M_V = -8.5$ (Saviane et al. 2003). At least the tip of the southern tail of NGC 4038/39 contains star clusters.

3.2. NGC 3256

NGC 3256 is intermediate in the Toomre sequence, and it is the second nearest merger in this study. The inner region has structures such as loops, knots, and dust lanes usually seen in mergers, as well as sweeping, symmetric tidal tails (see the optical image in Fig. 1). In radio continuum observations, two nuclei can be seen, separated by ~1 kpc (Norris & Forbes 1995). Of the Toomre sequence mergers, NGC 3256 has the most molecular gas, $1.5 \times 10^{10}\,M_\odot$ (Casoli et al. 1991; Aalto et al. 1991; Mirabel et al. 1990), and is the brightest in the far-infrared, with $L_{FIR} = 3 \times 10^{11}\,L_\odot$ (Sargent, Sanders, & Phillips 1989). In addition, NGC 3256 is the most X-ray luminous starburst known, with $L_{0.5-10\,keV} = 1.6 \times 10^{42}$ ergs s^{-1} (Moran, Lehnert, & Helfand 1999). The tails have rich H I content, but no tidal dwarf candidates have been discovered within them (see the H I contours in Fig. 1; English et al. 2003).

The approximate dynamical age of NGC 3256 is calculated in a similar manner as for NGC 4038/39 (presented in § 3.1). However, for a face-on orientation the maximum velocity is best represented by the escape velocity, 150 km s^{-1} (English & Freeman 2003), and the tail age is estimated to be 61 kpc/150 km s^{-1} = 400 Myr.

3.2.1. Inner Region

In WFPC2 images, Zepf et al. (1999) find more than 1000 compact, bright blue objects in the inner regions of NGC 3256. This population has colors, luminosities, and sizes similar to those of young globular clusters, with ages from a few to several hundred million years. The luminosity function can be fitted with a power law. The young cluster

population is quite extreme in that it comprises $\sim20\%$ of the total blue luminosity of the galaxy. This could indicate a high global efficiency of cluster formation.

3.2.2. Observations of the Western and Eastern Tails

In Figure 1, the WFPC2 field of view is overlaid on an optical image of NGC 3256. The V- and I-band images of the western tail were obtained on 1999 March 24, and we present the V-band image in Figure 3. The images of the eastern tail, obtained on 1999 October 11, are represented by the V-band image in Figure 4. The 50% and 90% completeness limits correspond to $M_V = -7.5$ and $M_V = -8.7$, respectively.

3.2.3. Results

The observations of the inner region from Zepf et al. (1999) were obtained in the B and I bands, which precludes a direct comparison with our observations in V and I. From the V-band WFPC2 images of the western and eastern tails in Figures 3 and 4, it can clearly be seen that the density of objects is higher within the tail regions. In addition, both the western and eastern tails show a grouping of sources in the CMD at $-10 < M_V < -7$ and $0 < V-I < 1$, which is more prominent in the in-tail than in the out-of-tail regions (see Fig. 11). For the western tail, the K-S statistic indicated that the probabilities that the magnitude and colors of in-tail and out-of-tail sources are drawn from the same population are 0.03 and 2.2×10^{-6}, respectively. For the eastern tail, the statistical significance of the difference is not as large. The magnitudes have a K-S probability of 0.20 of being drawn from the same distribution, but the color distributions are different at greater than $2\,\sigma$ significance. Some of the fainter sources could be individual stars, but the majority are likely to be clusters (Whitmore et al. 1999b). In the western tail, there are 71 sources falling in the region of the CMD defined by $-10 < M_V < -7$ and $0 < V-I < 1$. The eastern tail has 25 sources in this region. Outside the
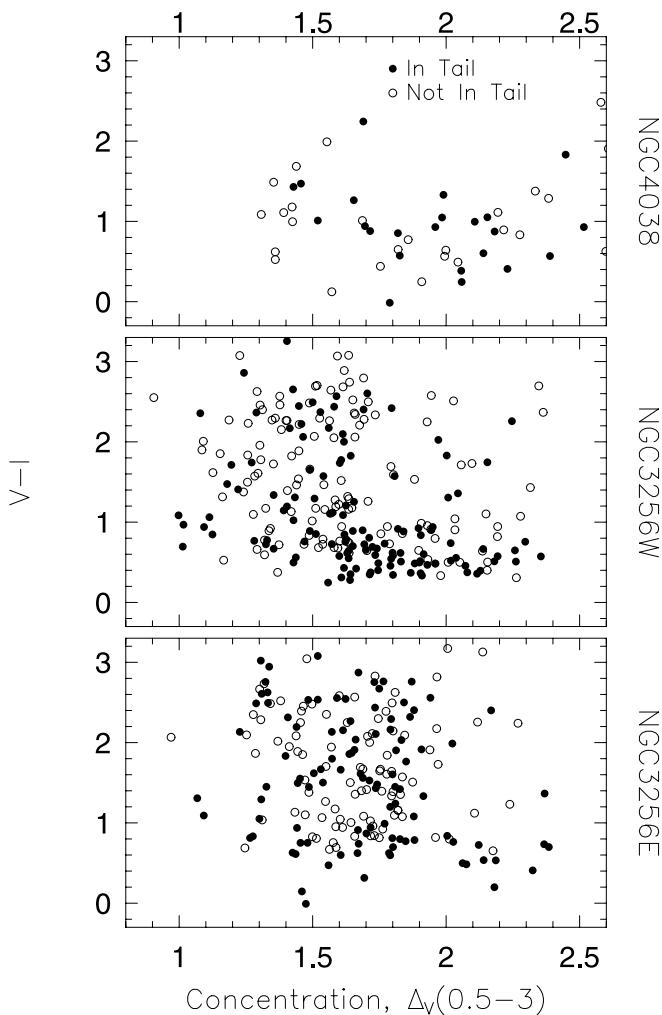
FIG. 10.—Concentration index plots for the two nearest mergers, NGC 4038 and NGC 3256 (western and eastern tails). Color $V-I$ is plotted vs. concentration index $\Delta_V (0.5 - 3)$. The concentration index (a rough measure of cluster size) was calculated from the difference in V magnitude between an aperture of 0.5 and 3.0 pixel radii. Sources within the tail (*solid circles*) and those outside (*open circles*) the tail are indicated.

tail, there are only 29 sources in the western image and eight in the eastern image that fall within this same region of the CMD.

The cluster candidate sample is contaminated by foreground stars since NGC 3256 is at a low Galactic latitude ($b = +11.7$). Examination of the concentration index can aid in separating the clusters from the stars. The concentration index for blue sources ($V-I < 1.1$) within the western tail (Fig. 10) is peaked at ~ 1.8, while for red sources ($V-I > 1.1$) out of the tail, the peak is ~ 1.5. Hence the clusters (blue objects) appear to be resolved compared to the stars (red objects). By the K-S test, these distributions have a probability of 0.06 of being drawn from the same distribution of concentration index, but the distribution of colors differs at greater than $5\,\sigma$. There is a grouping of sources in the concentration index plot at a large concentration index that is composed of the same sources as the grouping at $0 < V-I < 1$ in the CMD.

Candidate cluster sources in the eastern tail are less numerous than those in the western tail, but many of them are in the same region of the CMD and the concentration

index plot as those western sources that have been identified as clusters. In the western tail, there is a clear separation in concentration index between in-tail and out-of-tail sources. The sources in the eastern tail have less separation, no significant difference in the distribution of concentration index by the K-S statistic [P(K-S) = 0.84], and a $2\,\sigma$ difference in the distribution of color.

The majority of clusters in the eastern tail, 18 out of 25, appear in WF2, which includes the part of the tail closest to the center. In the western tail, the majority of clusters, 43 out of 71, appear in WF4, compared to 25 in WF2, the other significant contributor. In this case, WF4 contains the part of the tail farthest from the center.

3.2.4. *Discussion*

From the CMD (Fig. 11) and the concentration index diagram (Fig. 10) for the western tail, we infer that most of the sources with $-10 < M_V < -7$ and $0 < V-I < 1$ are star clusters. The peak of the color distribution is $V-I \sim 0.5$. The majority of clusters in the western tail are in the outer higher surface brightness regions of the tail.

There are fewer clusters in the eastern tail, and the majority of them are closer to the inner regions. The eastern tail appears to be of higher surface brightness toward the center, following the distribution of clusters. In addition to more star clusters, the western tail has a higher H I mass than the eastern tail ($2.2 \times 10^9\ M_\odot$ vs. $1.4 \times 10^9\ M_\odot$; English et al. 2003).

Ages of clusters can be estimated using the evolutionary tracks for a $10^5\ M_\odot$ instantaneous burst (Bruzual & Charlot 1993; Charlot, Worthey, & Bressan 1996)[5] with solar metallicity and a Salpeter initial mass function (IMF), superposed on the CMDs in Figure 11. A range of cluster masses, $\sim 10^4$–$10^5\ M_\odot$, would allow for a population with the range of ages, 30–300 Myr, to explain most of the observed M_V and $V-I$. However, the bluer clusters (those with $V-I < 0.3$) require either a lower metallicity (see Schweizer et al. 1996) or considerably younger populations (several million years old). Regardless, it would appear that the clusters are younger than the tail in which they formed. Therefore, they were not pulled out into the tail from inner regions, but rather they formed in situ in dense H I regions within the tail.

3.3. *NGC 3921*

NGC 3921, the second to last of the Toomre sequence, features a single nucleus, a main body with ripples and loops, and a pair of crossed tidal tails. The two galaxies have essentially merged (Fig. 1; see also Schweizer 1996). The southern tail extends below the main body, ending in a large concentration of H I, possibly a tidal dwarf galaxy (Hibbard & van Gorkom 1996). NGC 3921 is the most distant merger in our sample of four.

Consistent with an evolved merger, the optical spectrum is dominated by Balmer absorption lines, a classic post-starburst signature (Kennicutt 1992). NGC 3921 shows no H I in the northern tail, while the southern tail is gas-rich (see the H I contours in Fig. 1). This difference in H I between the tails may indicate the merger of two different types of galaxies, a gas-rich, late-spiral type and a gas-poor, early-type

---

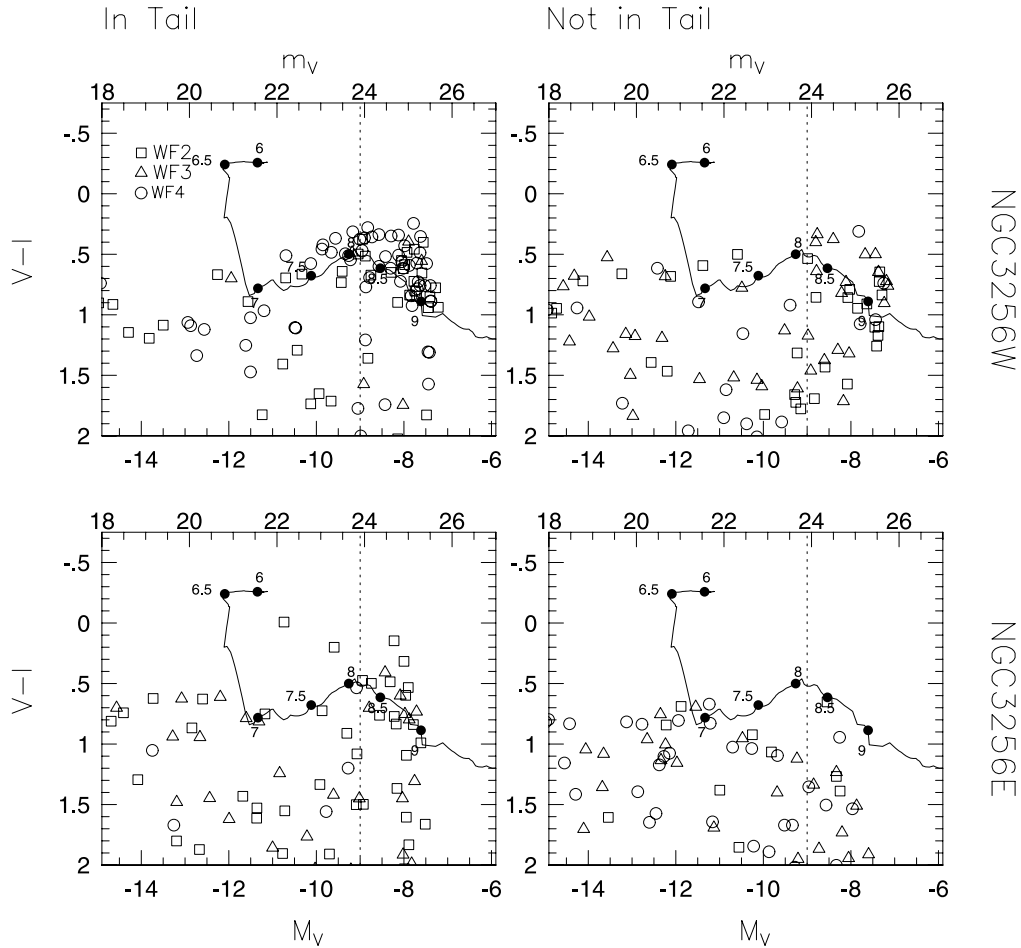[5] See http://www.stsci.edu/instruments/observatory/cdbs/cdbs_bc95.html.

Fig. 11.—Same as Fig. 9, but for NGC 3256. The western and eastern sources are given in the top and bottom rows, respectively.

disk galaxy. The approximate tail age of NGC 3921, calculated as in § 3.1, is 64 kpc/140 km s^{-1} = 460 Myr (Hibbard & van Gorkom 1996).

3.3.1. Inner Region

In WFPC2 images obtained by Schweizer et al. (1996), hereafter S96, there are two chains of pointlike candidate globular clusters and more extended stellar associations along the inner part of the southern tail, as well as several slender, narrow arcs of these sources. Their HST image reveals ~100 candidate globular clusters and ~50 stellar associations. The globular clusters tend to be more centrally located, while the associations trace the southern loop and two tidal tails.

The majority of the inner region's clusters and associations are blue and have rather uniform colors with a median V−I = 0.65 for globular clusters and 0.56 for associations. Depending on the metallicity, the ages of the globular clusters range from 250 to 750 Myr with an upper limit on their radii of 5 pc. The luminosity function of the globular clusters and that of the associations are represented by power laws. S96 estimate that the number of globular clusters increased by greater than 40% during the merger.

3.3.2. Observations of Southern Tail

In Figure 1, the WFPC2 field of view is overlaid on an optical image of NGC 3921 (see Table 1 for exposure infor-

mation). The images of the southern tail, obtained on 1999 April 30, are represented by the V-band image in Figure 5. With a distance modulus of 34.5 (for $H_0 = 75$ km s^{-1} Mpc^{-1}; S96), our source catalog for NGC 3921 is 50% complete to $m_V \sim 25.8$, consistent with our visual estimate of the completeness correction from the CMD, which at this large distance corresponds only to $M_V = -8.7$.

3.3.3. Results

Because our image partially overlaps with the observation by S96, we compare three globular cluster candidates and five stellar association candidates found in that paper, which correspond to our sources. These eight sources have a range in brightness of $23.5 < V < 25.4$ and a range in color of $-0.2 < V-I < 1.1$. The mean difference between the S96 data and our data is 0.12 mag for $V-I$ and 0.43 mag for V. The S96 values are consistently fainter than our values and slightly redder on average. The differences between the data appear to be due to the differences in the corrections for finite aperture size, CTE, and reddening. For sources on the WF chips, S96 used a 1 pixel aperture for aperture photometry, while our procedure used a 2 pixel aperture. This would cause more extended sources, or stellar associations, to have a larger difference between the two data sets than the less extended sources since a single aperture correction has been made for all sources. In our comparison, the five associations have a mean difference of 0.55 mag in V and
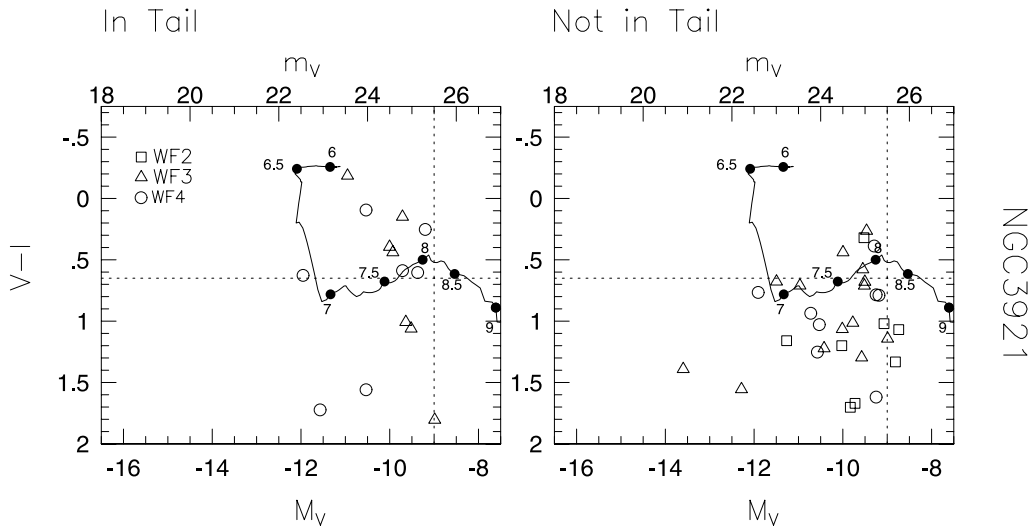
In Tail　　　　　　　　　　　　　Not in Tail

FIG. 12.—Same as Fig. 9, but for NGC 3921. The horizontal line represents the median $V-I$ for the clusters in the inner region of the merger.

0.12 mag in $V-I$, while the cluster candidates have a mean difference of 0.23 mag in V and 0.09 mag in $V-I$. Corrections for CTE problems were not made by S96 because of the varied backgrounds in their images. Our calculations include corrections for CTE, at times as large as -0.2 mag for faint sources near the top of the chip. S96 used $A_V = 0.00$ to correct for foreground Milky Way extinction, whereas we used $A_V = 0.046$. As an independent check on their photometry, S96 compared their photometry performed with VISTA software with photometry using IRAF software. The objects measured in IRAF were found to have a mean difference in $V-I$ of 0.08 mag bluer than the objects measured in VISTA, possibly because of different centering algorithms or different aperture corrections. Regarding V magnitudes, S96 estimated that larger associations may have V magnitudes up to several tenths of a magnitude brighter, due to their more extended profile. Hence, taking into account differences in corrections for aperture size, CTE, and reddening, we find our values for photometry to be consistent with the S96 photometry.

As shown in Figure 12, there are few sources seen in the tail of this system. S96 found a population of bright clusters in the inner region with a narrow color range at $V-I = 0.65$, indicated by the horizontal dotted line in Figure 12. Sources in the tail do not appear to be clustered around this line, indicating that there is not a large population of clusters of the same age in the tail. The K-S test shows no significant difference between the distributions of color and magnitude $[P(\text{K-S}) = 0.98$ and $0.05]$ for sources in the tail compared with those out of the tail.

The associations that overlap with S96 fall in the same region of the CMD, $-11 < M_V < -9$ and $-0.1 < V-I < 0.9$. There are a few additional sources in the tail that also fall in this region of the CMD, and most of these lie closer to the inner region of the merger.

In a first pass through the photometry, only point sources were kept, using the method outlined in § 2.4. This method yielded very few sources and missed several of the associations identified in S96. When the criteria were relaxed, as outlined in § 2.2, many more extended objects were found. Most of those found out of the tail may be background galaxies, but those within the tail have properties consistent

with the stellar associations found in S96. At this distance one WF pixel corresponds to 39 pc, so it is difficult to distinguish clusters from stars using the concentration index.

The putative tidal dwarf galaxy was imaged in the PC. It appears to be a low surface brightness dwarf, and no point sources were found within it. However, there are four knots within the more diffuse emission, which extends over about 7 kpc. This tidal dwarf galaxy candidate will be addressed in a future study of the extended sources within these tails.

3.3.4. *Discussion*

Most of our sources that are in the same region of the CMD as those from S96 are located in the region closer to the main body of the merger and are bluer than sources elsewhere in the field. Most of the bluer sources in the tail have a large concentration index, indicating the possible presence of larger stellar associations. In addition to these large associations, there is a putative dwarf galaxy centered in the PC. There is an absence of point sources in the optical tail at larger distances from the main body of the merger.

3.4. *NGC 7252 (Atoms for Peace)*

As the system located at the end of the Toomre sequence, NGC 7252 exemplifies the prototypical merger remnant (see the optical image in Fig. 1). It is the second most distant of the four mergers in our sample. Schweizer (1978, 1998) defines some characteristics of a recent merger remnant: a pair of long tidal tails, isolated from neighbors, a single nucleus, tails moving in opposite directions relative to nucleus, and chaotic motions in the main body of the merger, all of which NGC 7252 possesses (Schweizer 1982). The central region of this remnant has a single nucleus with several loops. Observations with the *HST* have revealed a minispiral structure in the inner region that coincides with the disk of molecular and ionized gas (Wang, Schweizer, & Scoville 1992; Whitmore et al. 1993; Miller et al. 1997). The long, straight tails extend from the body of the remnant to the east and northwest, each ending in a concentration of H I associated with a candidate tidal dwarf galaxy. The outer parts of both tails have blue $B-R$ colors, with the

bluest parts coincident with the highest gas density (Hibbard et al. 1994).

The tails of NGC 7252 and the western-loop region are both rich in H I (see the H I contours in Fig. 1). The kinematics of the northwestern tail suggest that the material at the base of the tail is falling into the main remnant (Hibbard & Mihos 1995). This infall could explain some of the peculiar ripples and shells associated with the center. The presence of a young, metal-poor emission line cluster in the western loop (15 kpc from the center) is consistent with recent star formation that is perhaps triggered by infalling metal-poor gas from the tail (Schweizer & Seitzer 1998). The approximate tail age of NGC 7252, calculated as in § 3.1, is 160 kpc/220 km s^{-1} = 730 Myr (Hibbard et al. 1994), which is in good agreement with the age of 770 Myr as determined through numerical modeling (Hibbard & Mihos 1995; correcting to $H_0 = 75$ km s^{-1} Mpc^{-1}).

3.4.1. *Inner Region*

WFPC2 observations of the inner regions of NGC 7252 detected ∼500 cluster candidates that separate into three populations. Luminous blue clusters, with a narrow color range $V-I \sim 0.65$, have ages around 650–750 Myr. They were likely to have formed around the time that the tails were launched. These clusters have an upper size limit of 4.8 ± 0.4 pc. The inner disk is home to a population of very young (∼10 Myr) clusters, with $U-B$ colors indicating that O stars dominate and with radii of 8.3 ± 0.6 pc. The third population consists of the older, metal-poor globular clusters from the original galaxies. The combined luminosity function of these populations of clusters is a power law with $\alpha \sim -1.8$ (Miller et al. 1997).

3.4.2. *Observations of Western and Eastern Tails*

In Figure 1, the WFPC2 fields of view are overlaid on an optical image of NGC 7252 (see Table 1 for exposure information). The images of the western tail, obtained on 1998 November 18, are represented by the V-band image in Figure 6. The eastern tail observations, obtained on 1999 August 29, are represented by the V-band image in Figure 7. With a distance modulus of 34.0 (for $H_0 = 75$ km s^{-1} Mpc^{-1}; Schweizer 1982), the detection limit of $m_V \sim 26.0$ (50% completeness), consistent with our visual estimate of the completeness correction from the CMDs, corresponds to $M_V = -8.1$.

3.4.3. *Results*

The clusters in the inner region identified by Miller et al. (1997) include populations of intermediate and old clusters at $V-I = 0.65$ and 1.0, as indicated by the horizontal dotted lines on the CMD in Figure 13. The blue clusters have $19 < V < 25$. There are also some bright blue clusters with $V-I < 0.6$ (Miller et al. 1997), found mostly within the inner 6″ of the galaxy.

The western-tail CMD shows a possible enhancement of bluer faint sources at $-12 < M_V < -8.5$ and $0.2 < V-I < 1.0$ (Fig. 13), which are located in the tail region. The K-S test yields a difference at a 2 σ level between the colors for in-tail and out-of-tail sources, but no significant difference in their magnitude distributions. Seven members of the group at $0.2 < V-I < 0.65$, noted as star-shaped symbols on the CMD, are located in the putative tidal dwarf galaxy. A close-up of the V-band image of this region with the seven star clusters indicated is shown in Figure 14. The several sources with $0.65 < V-I < 1.0$ are spread through the optical tail.

For the eastern tail, Figure 13 shows a small group of sources in the tail at $M_V \sim -9$ and $0.2 < V-I < 1.2$. However, this concentration is not different from the grouping in the CMD of sources not in the tail. There is only one bright candidate ($M_V < -9$) in the tail region, while the region outside the tail hosts several such bright sources at $V-I \sim 0.5$. The nature of these sources is ambiguous. The K-S statistic shows no significant difference in either the magnitude or the color distributions for in-tail and out-of-tail sources. The concentration index is less useful for this merger because it is so far away (1 WF pixel is 31 pc). There are two sources in the eastern-tail dwarf that are quite blue ($V-I < 0.3$), noted as three-pointed symbols on Figure 13; see Figure 14 for a V-band image of the dwarf.

3.4.4. *Discussion*

Although there are several blue sources with $V-I < 1.0$ in the eastern- and western-tail regions, there is no convincing evidence for an excess over the out-of-tail regions, with the important exception of clusters within the prominent tidal dwarf candidates in each tail.

The tidal dwarf candidate in the western tail is clumpy, consisting of several knots spread over ∼1 kpc and embedded in extended high surface brightness material. There are seven clusters found within it, and they are relatively blue. Their concentration indices are somewhat larger (2.2–3.0) than the mean of 1.8 for the tidal cluster sources, but they are still consistent with being clusters at this distance. However, the measurement of the concentration parameters for clusters in this tidal dwarf candidate is uncertain since it is a crowded environment. These clusters in the western tidal dwarf candidate are grouped together in the CMD (star-shaped symbols in Fig. 13) and their average $V-I$ color is 0.4, bluer than the major population of clusters in the inner regions of NGC 7252. The CMD suggests an age of less than 100 Myr, which is less than the formation age of the tail, and as such the clusters formed within the tidal debris.

Hibbard et al. (1994) found strong kinematic evidence for a mass concentration at the location of the putative tidal dwarf in the western tail of NGC 7252. This evidence consisted of an increase in the H I line width centered on and symmetric with the concentration of gas, light, and star-forming regions associated with the tidal dwarf galaxy. The appearance of star clusters at this location, especially since there is no statistically significant excess of star clusters elsewhere in the tail, is further evidence in support of this region being dynamically distinct.

The tidal dwarf in the eastern tail is almost featureless and of only slightly higher surface brightness than the tail. The several clusters within the dwarf are among the bluest in the sample. They are consistent with the very blue colors of those clusters within the inner 6″ of NGC 7252. These inner region clusters have an age of ∼10 Myr. Though the clusters could have formed recently, the dwarf itself may have formed earlier.

The contrast in the distribution of young stars in the two candidate dwarf galaxies is striking. The western-tail dwarf is of higher surface brightness and contains several blue clusters in close proximity, and the eastern-tail dwarf is
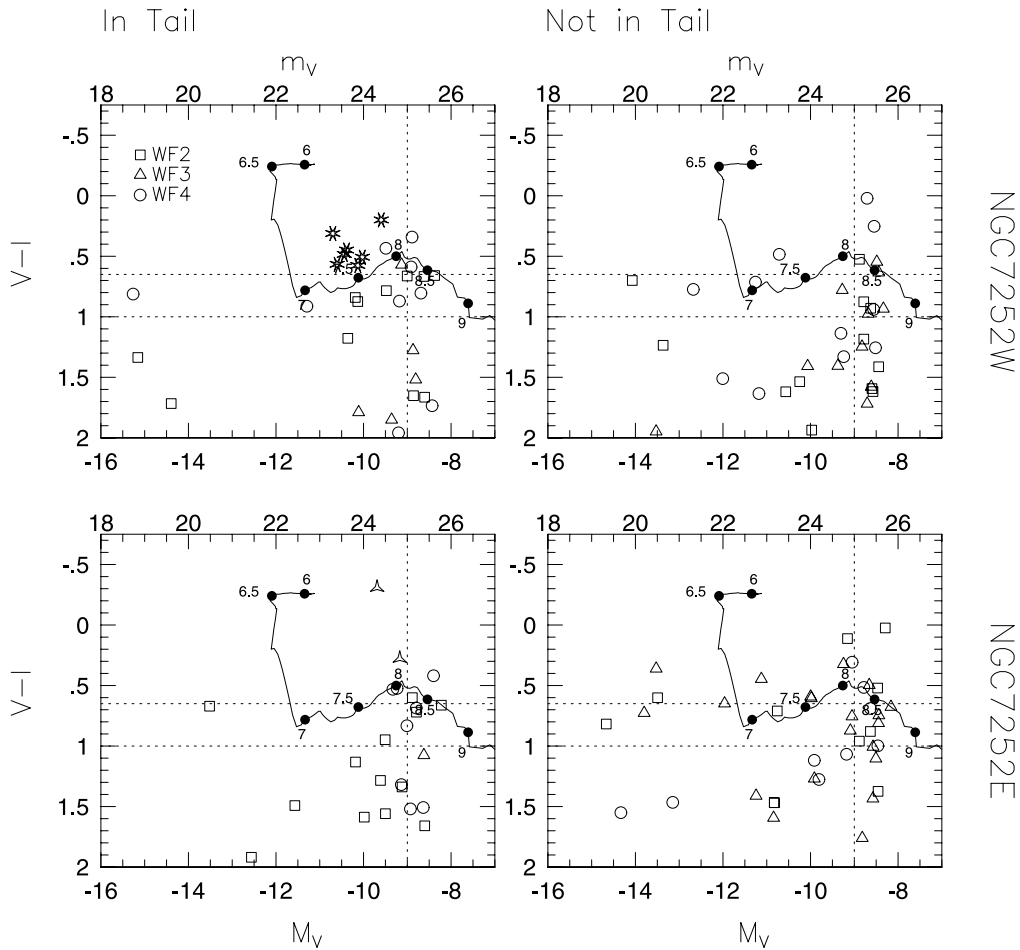
FIG. 13.—Same as Fig. 9, but for NGC 7252. The western and eastern sources are given in the top and bottom rows, respectively. The sources in the tidal dwarfs at the end of the western and eastern tails (see Fig. 14) are indicated as symbols of the shape corresponding to the appropriate WF chip. For comparison, the horizontal dotted lines represent the colors of the two main populations of clusters in the inner region of this merger. The evolutionary track for a single burst Bruzual and Charlot model (Bruzual & Charlot 1993) is given as in previous CMDs.

almost featureless, with only two clusters spaced farther apart. In the eastern-tail dwarf, the extreme blue colors indicate that the clusters are considerably younger than the age of the interaction. A similar situation is found in the northern starburst region of Stephan's Quintet, one of Hickson's compact galaxy groups. That region is separated from the nearest giant galaxy by more than 25 kpc, yet it hosts a very young stellar population (less than 5 Myr; Gallagher et al. 2001). It will be interesting to compare the range of properties of these and other tidally formed dwarfs to the varied population of compact and diffuse dwarf galaxies in the Local Group.

4. SUMMARY AND DISCUSSION

In our study of six *HST* WFPC2 images of six tidal tails in four merging pairs, we found evidence of extreme differences in cluster formation among the tidal tails. To compare the debris in the different mergers on an equal footing, we must consider contamination by foreground and background objects and the relative areas of in-tail and out-of-tail regions (fractions f_{in} and f_{out}). We must also consider selection effects due to the different distances of the pairs. Table 3 gives the in-tail and out-of-tail source densities in each tidal tail for sources with $V-I < 0.7$ and with

$M_V < -8.5$. The latter criterion was chosen because sources this bright are likely to be clusters rather than individual stars. Table 3 also lists the specific frequencies of young clusters, S_{young}, for each tail region, defined as the number of young clusters per $M_V = -15$ luminosity (similar to the way Harris 1991 defined the specific frequency for old globular clusters).

Figure 15 gives, for the six regions, the differences in the source densities in and out of the tails. This is a way of subtracting the background, but it neglects the fact that some out-of-tail sources might be real clusters. Error bars are simply from Poisson statistics; if some of the objects outside of the tails are clusters, then the background subtraction is systematically too large and the surplus found would represent a lower limit.

The western-tail region of NGC 3256 shows a significant excess of sources likely to be star clusters. The five other regions show a much smaller number, consistent with zero for NGC 4038 and NGC 7252E, but statistically significant for the other three tail regions, NGC 3256E, NGC 3921, and NGC 7252W. In the case of NGC 3921, many of the sources in the southern tail are stellar associations also reported by S96. By having different detection criteria for NGC 3921 and NGC 7252, we attempted to find any faint clusters that might add to the numbers such that these
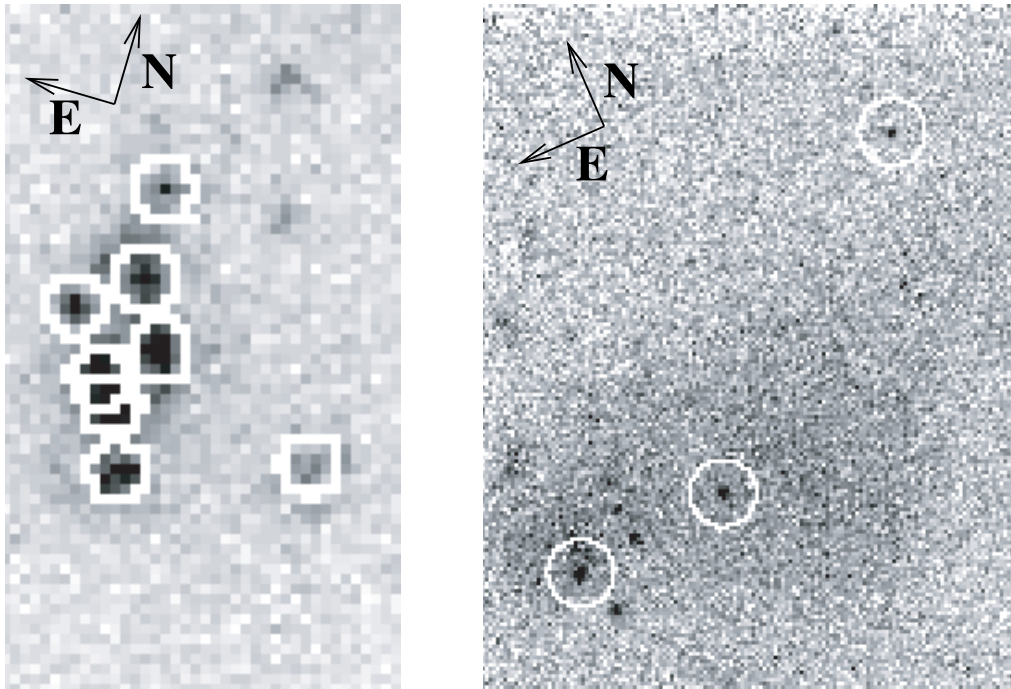
Fig. 14.—Dwarf galaxies at the ends of the western (*left*) and eastern (*right*) tails of NGC 7252, taken in the F555W (*V*) filter. The colors and magnitudes of several clusters within these dwarfs are shown as star-shaped symbols in the CMDs of Fig. 13. The clusters in the western dwarf are found to be relatively blue ($V-I \sim 0.4$), somewhat younger than the dominant population in the inner region, which has an age of $\sim$650–750 Myr. Those in the eastern tail are extremely blue ($V-I < 0.3$), consistent with the youngest population in the inner regions, having an age of $\sim$10 Myr.

regions might compete with the number of clusters found in NGC 3256W. Since we did not find a population of faint sources in the tails of NGC 3921 and NGC 7252, the excess of sources in NGC 3256W is even more significant. If we look at just the brightest sources in all the tails that have $M_V < -9.0$ and $M_V < -9.5$ (with $V-I < 0.7$, as above), NGC 3256W still has a much larger excess of clusters within the tail.

While the tails of NGC 7252 generally lack clusters, it is remarkable that there is a population of clusters associated with both tidal dwarf candidates (seven in the western dwarf, two in the eastern one). The two tidal dwarf candidates show different populations of clusters, however, with the eastern dwarf bluer than the western dwarf. For the western tidal dwarf, the clusters may have formed either before or concurrent with the dwarf. The eastern dwarf probably formed prior to its recent burst of star formation. Though differential reddening could induce the observed color differences between the two dwarfs, we have no evidence that suggests this might be the case.

The NGC 4038 tidal debris shows no large young cluster population like that observed in its inner regions. There are fainter objects, which could be individual young stars within the tail, but there are only three objects brighter than $M_V = -9$, the cutoff for clusters used by Whitmore et al. (1999b), and all of these have $V-I > 1$. At least this section of the tail, if not the entire tail, has few, if any, clusters. Interestingly, *HST* WFPC2 images of the region of the tail coincident with the tidal dwarf candidate (Saviane et al. 2003) show eight young stellar associations in the vicinity of the tidal dwarf. The high concentration of blue star clusters in the vicinity of a tidal dwarf candidate, but general lack of such clusters elsewhere in the tail, is very similar to the situation for NGC 7252. It will be very interesting to see if the other two unreduced pointings on the NGC 4038/39 tails (see Fig. 1) show a similar lack of bright clusters.

Clearly, the western tail of NGC 3256 has the largest population of tail clusters observed in our sample. Both the colors and concentration of these objects are coincident

TABLE 3
SOURCE DENSITIES IN AND OUT OF DEBRIS

| Tidal Tail	Pixel Size (pc)	N_{out}	f_{out}	N_{out}/Area (kpc^{-2})	N_{in}	f_{in}	N_{in}/Area (kpc^{-2})	Surplus	Specific Frequency
NGC 4038..................	8.92	1	0.501	0.013 ± 0.013	1	0.499	0.013 ± 0.013	0.000 ± 0.018	0.0
NGC 3256W	18.2	12	0.677	0.028 ± 0.008	28	0.323	0.136 ± 0.026	0.108 ± 0.027	2.5
NGC 3256E	18.2	4	0.538	0.012 ± 0.006	9	0.462	0.031 ± 0.010	0.019 ± 0.012	0.4
NGC 3921S................	38.8	7	0.751	0.003 ± 0.001	9	0.249	0.013 ± 0.004	0.010 ± 0.004	0.2
NGC 7252W	31.1	5	0.623	0.004 ± 0.002	13	0.377	0.019 ± 0.005	0.015 ± 0.005	1.1
NGC7252E................	31.1	13	0.618	0.011 ± 0.003	7	0.382	0.010 ± 0.004	-0.001 ± 0.005	-0.2
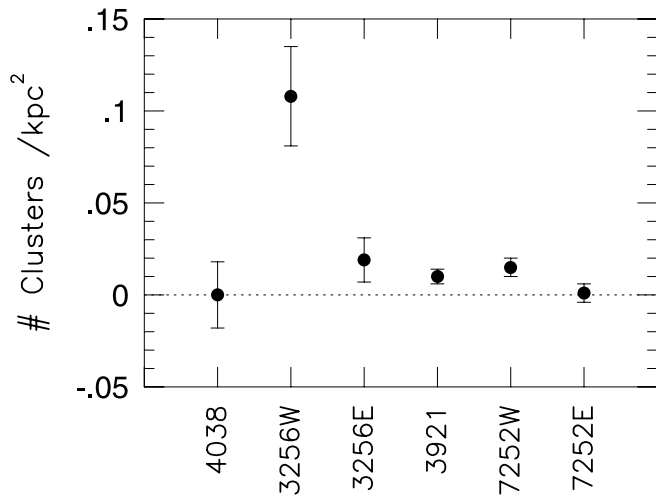
FIG. 15.—Number of candidate clusters per square kiloparsec compared for the six different areas of debris. Background sources were subtracted, statistically, using the source densities in areas outside of the tail. The excesses in the tail are plotted. Details of the calculation are given in Table 3.

with inner region clusters in the merger. The eastern tail has a small excess ($\sim 2\,\sigma$) of clusters as well.

So why might the tails of NGC 3256 be a preferred environment for extensive cluster formation? The tails of NGC 3256 are very similar to other tails that do not show such large numbers of clusters; all show large numbers of inner region clusters; all are rich in atomic gas; all have dynamical ages ranging from 400 to 800 Myr (with NGC 3256 and NGC 3921 at the lower range of that scale). However, NGC 3256 is extremely bright in the X-ray and far-IR and also has the largest number of clusters in its inner regions.

From the far infrared luminosities of each pair, we calculated the global star formation rates using the relation of Kennicutt (1998): SFR $= 4.5 \times 10^{-44} L_{\rm FIR}\ M_\odot\ {\rm yr}^{-1}$. This conversion assumes that the dust re-emits all of the young starlight ($\tau \gg 1$) and that the dust heating is dominated by young stars, with ages on the order of 10^8 yr or less. As shown in Table 4, NGC 3256 stands out clearly with a star formation rate several times that of the Antennae and NGC 7252, the next closest pairs. Although these rates are calculated from the integrated infrared luminosities rather than locally for the tidal tails, the overall enhancement of star formation in NGC 3256 may be a prerequisite for the efficient production of star clusters. Also, the star formation rate is related to the current burst of star formation and might not indicate the conditions in the merger when the star clusters in the tails formed, but perhaps the higher star formation rate of NGC 3256 indicates a higher global molecular gas content that would aid in more efficient star cluster formation.

We should consider whether the specific frequency of young clusters is large for NGC 3256, or whether the number of young clusters is what would be expected based on the luminosity of the tail region. From Whitmore & Schweizer (1995) and Goudfrooij et al. (2001), we can compare the specific frequency of young clusters forming in the central regions of mergers with $S_{\rm young}$ of our tidal tails. We calculated the M_V of the tidal tails by using the IRAF task IMSTAT at several typical locations within the tail and subtracted the background, measured at several locations outside the tail. The western tail of NGC 3256 has a very large specific frequency, $S_{\rm young} = 2.5$, comparable to $S_{\rm young} \sim 2$[6] found in the central regions of NGC 4038/39 (Whitmore & Schweizer 1995) and $S_{\rm young} = 1.7$[7] found in NGC 1316 (Goudfrooij et al. 2001). Clearly, the calculation of $S_{\rm young}$ is complicated by the destruction of clusters, fading, etc. However, it is still quite interesting that one of these tails hosts clusters that are as luminous, relative to stars, as in central regions of merging galaxies.

Another difference between NGC 3256 and the other pairs, is that, unlike the other three systems, NGC 3256 does not have a prominent tidal dwarf galaxy associated with the tip of its tidal tail either in the optical image or in H I maps. A hypothesis, based on our admittedly small sample of six tidal tails, is that tails with prominent tidal dwarfs form fewer clusters than tails without such dwarfs. If we also consider the ACS early release observations of UGC 10214 and NGC 4676, they follow a similar trend. Although no correction was made for background contamination, UGC 10214 (which has a tidal dwarf candidate) has fewer star clusters in its tail than NGC 4676 (which does not host a tidal dwarf candidate; de Grijs et al. 2003; Tran et al. 2003). However, UGC 10214 is thought to be a disturbed spiral with a single long tidal tail, a different environment from the merging pairs of spiral galaxies that comprise our sample and NGC 4676. UGC 10214 also hosts many young star clusters in the bright blue clump at the midpoint of its tail with ages from ~ 3 to 10 Myr (Tran et al. 2003).

Elmegreen & Efremov (1997) showed that large mass clumps and high specific kinetic energies lead to a higher efficiency for star formation because of an increased binding energy and resistance to disruption. Perhaps the details of the interaction (i.e., the mass of the perturber, the orbital properties of the two galaxies as they merge, the gas content of the parent galaxy, the dark matter distribution, and the velocity of the perturber) influence the process of star formation in the debris. We hypothesize that global characteristics of the encounters affect the local conditions, conspiring so that star clusters form along the tail or within a dwarf galaxy in the tail, but not both.

TABLE 4
STAR FORMATION RATES OF MERGING PAIRS

Pair	$F_{\rm FIR}$ (ergs cm^{-2} s^{-1})	SFR ($M_\odot$ yr^{-1})
NGC 4038/39[a]	2.6×10^{-9}	5.2
NGC 3256[b]	4.32×10^{-9}	33.4
NGC 3921[b]	$(2.69–5.25) \times 10^{-11}$	1.9
NGC 7252[c]	2.37×10^{-10}	5.4

[a] From Ranalli, Comastri, & Setti 2003.
[b] From Moshir et al. 1990.
[c] From Knapp et al. 1989.

[6] In this expression $S_{\rm young}$ corresponds to S in Whitmore & Schweizer (1995).
[7] In this expression $S_{\rm young}$ corresponds to S_N in Goudfrooij et al. (2001).

REFERENCES

Aalto, S., Black, J. H., Booth, R. S., & Johansson, L. E. B. 1991, A&A, 247, 291
Ajhar, E. A., Blakeslee, J. P., & Tonry, J. L. 1994, AJ, 108, 2087
Amram, P., Marcelin, M., Boulesteix, J., & le Coarer, E. 1992, A&A, 266, 106
Barnes, J. E. 1988, ApJ, 331, 699
Barth, A. J., Ho, L. C., Filippenko, A. V., & Sargent, W. L. W. 1995, AJ, 110, 1009
Bruzual, A. G., & Charlot, S. 1993, ApJ, 405, 538
Casoli, F., Dupraz, C., Combes, F., & Kazes, I. 1991, A&A, 251, 1
Charlot, S., Worthey, G., & Bressan, A. 1996, ApJ, 457, 625
de Grijs, R., Lee, J. T., Mora Herrera, M. C., Fritze-v. Alvensleben, U., & Anders, P. 2003, NewA, 8, 155
Duc, P.-A., & Mirabel, I. F. 1994, A&A, 289, 83
———. 1998, A&A, 333, 813
———. 1999, in IAU Symp. 186, Galaxy Interactions at Low and High Redshift, ed. D. Sanders & J. Barnes (Dordrecht: Kluwer), 61
Elmegreen, B. G., & Efremov, Y. N. 1997, ApJ, 480, 235
English, J., & Freeman, K. C. 2003, AJ, 125, 1124
English, J., Norris, R. P., Freeman, K. C., & Booth, R. S. 2003, AJ, 125, 1134
Fritze-v. Alvensleben, U. 1998, A&A, 336, 83
Gallagher, S. C., Charlton, J. C., Hunsberger, S. D., Zaritsky, D., & Whitmore, B. C. 2001, AJ, 122, 163
Goudfrooij, P., Alonso, M. V., Maraston, C., & Minniti, D. 2001, MNRAS, 328, 237
Harris, W. E. 1991, ARA&A, 29, 543
Harris, W. E., & Pudritz, R. E. 1994, ApJ, 429, 177
Hibbard, J. E., Guhathakurta, P., van Gorkom, J. H., & Schweizer, F. 1994, AJ, 107, 67
Hibbard, J. E., & Mihos, J. C. 1995, AJ, 110, 140
Hibbard, J. E., van der Hulst, T., Barnes, J. E., & Rich, R. M. 2001a, AJ, 122, 2969
Hibbard, J. E., & van Gorkom, J. H. 1996, AJ, 111, 655
Hibbard, J. E., van Gorkom, J. H., Rupen, M. P., & Schiminovich, D. 2001b, in ASP Conf. Ser. 240, Gas and Galaxy Evolution, ed. J. E. Hibbard, M. P. Rupen, & J. H. van Gorkom (San Francisco: ASP), 659
Holtzman, J. A., Burrows, C. J., Casertano, S., Hester, J. J., Trauger, J. T., Watson, A. M., & Worthey, G. 1995, PASP, 107, 1065
Holtzman, J. A., et al. 1992, AJ, 103, 691
Hunsberger, S. D., Charlton, J. C., & Zaritsky, D. 1996, ApJ, 462, 50
Iglesias-Páramo, J., & Vílchez, J. M. 2001, ApJ, 550, 204
Jog, C. J., & Solomon, P. M. 1992, ApJ, 387, 152
Kennicutt, R. C. 1992, ApJ, 388, 310
———. 1998, in Galaxies: Interactions and Induced Star Formation, ed. R. C. Kennicutt, Jr., F. Schweizer, J. E. Barnes, D. Friedli, L. Martinet, & D. Pfenniger (Berlin: Springer), 1
Knapp, G. R., Guhathakurta, P., Kim, D., & Jura, M. A. 1989, ApJS, 70, 329
Kundu, A., & Whitmore, B. C. 2001a, AJ, 121, 2950
———. 2001b, AJ, 122, 1251
Larsen, S. S., & Richtler, T. 1999, A&A, 345, 59
Lee, H., Lee, Y., & Gibson, B. K. 2002, AJ, 124, 2664
Mathis, J. S. 1990, ARA&A, 28, 37
Meurer, G. R., Heckman, T. M., Lietherer, C., Kinney, A., Robert, C., & Garnett, D. R. 1995, AJ, 110, 2665

Miller, B., Whitmore, B., Schweizer, F., & Fall, S. M. 1997, AJ, 114, 2381
Mirabel, I. F., Booth, R. S., Johansson, L. E. B., Garay, G., & Sanders, D. B. 1990, A&A, 236, 327
Mirabel, I. F., Dottori, H., & Lutz, D. 1992, A&A, 256, L19
Moran, E. C., Lehnert, M. D., & Helfand, D. J. 1999, ApJ, 526, 649
Moshir, M., et al. 1990, IRAS Faint Source Catalog (ver. 2.0) (Greenbelt: NASA GSFC)
Norris, R. P., & Forbes, D. A. 1995, ApJ, 446, 594
Peterson, C. J. 1993, in ASP Conf. Ser. 50, Structure and Dynamics of Globular Clusters, ed. S. G. Djorgovsky & G. Meylan (San Francisco: ASP), 337
Press, W. H., Flannery, B. P., Teukolsky, S. A., & Vetterling, W. T. 1986, Numerical Recipes: The Art of Scientific Computing (Cambridge: Cambridge Univ. Press)
Ranalli, P., Comastri, A., & Setti, G. 2003, A&A, 399, 39
Reed, B. C., Hesser, J. E., & Shawl, S. J. 1988, PASP, 100, 545
Sargent, A. I., Sanders, D. B., & Phillips, T. G. 1989, ApJ, 346, L9
Saviane, I., Hibbard, J. E. & Rich, R. M. 2003, AJ, submitted
Schlegel, D. J., Finkbeiner, D. P., & Davis, M. 1998, ApJ, 500, 525
Schombert, J. M., Wallin, J. F., & Struck-Marcell, C. 1990, AJ, 99, 497
Schweizer, F. 1978, in Structure and Properties of Nearby Galaxies, ed. E. M. Berkhuijsen & R. Wielebinski (Dordrecht: Reidel), 279
———. 1982, ApJ, 252, 455
———. 1996, AJ, 111, 109
———. 1998, in Galaxies, Interactions and Induced Star Formation, ed. R. C. Kennicutt, Jr., F. Schweizer, J. E. Barnes, D. Friedli, L. Martinet, & D. Pfenniger (Berlin: Springer)
Schweizer, F., Miller, B., Whitmore, B., & Fall, S. M. 1996, AJ, 112, 1839 (S96)
Schweizer, F., & Seitzer, P. 1998, AJ, 116, 2206
Tran, H. D., et al. 2003, ApJ, 585, 750
Toomre, A. 1977, in The Evolution of Galaxies and Stellar Populations, ed. B. M. Tinsley & R. B. Larson (New Haven: Yale Univ. Press), 401
Toomre, A., & Toomre, J. 1972, ApJ, 178, 623
van den Bergh, S. 1996, AJ, 112, 2634
van der Hulst, J. M. 1979, A&A, 155, 151
Voit, M. 1997, HST Data Handbook (Baltimore: STScI)
Wang, Z., Schweizer, F., & Scoville, N. Z. 1992, ApJ, 396, 510
Weilbacher, P. M., Duc, P.-A., & Fritze-v. Alvensleben, U. 2003, A&A, 397, 545
Weilbacher, P. M., Duc, P.-A., Fritze-v. Alvensleben, U., Martin, P., & Fricke, K. J. 2000, A&A, 358, 819
Whitmore, B. C., Heyer, I., & Casertano, S. 1999a, PASP, 111, 1559
Whitmore, B. C., Miller, B. W., Schweizer, F., & Fall, S. M. 1997, AJ, 114, 1797
Whitmore, B. C., & Schweizer, F. 1995, AJ, 109, 960
Whitmore, B. C., Schweizer, F., Leitherer, C., Borne, K., & Robert, C. 1993, AJ, 106, 1354
Whitmore, B. C., Sparks, W. B., Lucas, R. A., Macchetto, F. D., & Biretta, J. A. 1995, ApJ, 454, L73
Whitmore, B. C., Zhang, Q., Leitherer, C., Fall, S. M., Schweizer, F., & Miller, B. 1999b, AJ, 118, 1551
Yun, M. S., Ho, P. T. P., & Lo, K. Y. 1994, Nature, 372, 530
Zepf, S., Ashman, K., English, J., Freeman, K., & Sharples, R. 1999, AJ, 118, 752
Zhang, Q., & Fall, S. M. 1999, ApJ, 527, L81